ENVIRONMENTAL RESEARCH
CLIMATE

PURPOSE-LED PUBLISHING™ Part of the ENVIRONMENTAL RESEARCH SERIES

PAPER • OPEN ACCESS

Heat vulnerability in a hyper-arid coastal conurbation: downscaled LST and socio-spatial analysis

To cite this article: Pablo Sarricolea *et al* 2025 *Environ. Res.: Climate* **4** 045017

ENVIRONMENTAL RESEARCH
CLIMATE

OPEN ACCESS

RECEIVED
26 June 2025

REVISED
13 October 2025

ACCEPTED FOR PUBLICATION
4 November 2025

PUBLISHED
21 November 2025

PAPER

Heat vulnerability in a hyper-arid coastal conurbation: downscaled LST and socio-spatial analysis

Pablo Sarricolea[1,2,*], Alexis Baltazar[1], Oliver Meseguer-Ruiz[3], Pamela Smith[1,2], Natasha Picone[4,5], Roberto Serrano-Notivoli[6], Paulina Vidal-Paez[7], Magdalena Fuentealba[8,9,10] and Felipe Thomas[1]

[1] Department of Geography, University of Chile, Portugal 84, Torre Chica, Santiago, Chile
[2] Center for Climate and Resilience Research (CR)[2], Santiago, Chile
[3] Departamento de Ciencias Históricas y Geográficas, Universidad de Tarapacá, Av. 18 de Septiembre 800, 100069 Arica, Chile
[4] Instituto de Geografía, Historia y Ciencias Sociales, CONICET—Universidad Nacional del Centro de la Provincia de Buenos Aires, Tandil, Argentina
[5] Centro de Investigaciones Geográficas, Facultad de Ciencias Humanas, Universidad Nacional del Centro de la Provincia de Buenos Aires, Tandil, Argentina
[6] Departamento de Geografía y Ordenación del Territorio, Instituto Universitario de Ciencias Ambientales (IUCA), Universidad de Zaragoza, Pedro Cerbuna 12, 50009 Zaragoza, Spain
[7] Hémera Centro de Observación de la Tierra, Escuela de Ingeniería Forestal, Facultad de Ciencias, Ingeniería y Tecnología, Universidad Mayor, Santiago, Chile
[8] Institute of Geography, Pontificia Universidad Católica de Chile, Vicuña Mackenna, 4860 Santiago, Chile
[9] Centro UC Desierto de Atacama, Pontificia Universidad Católica de Chile, Santiago, Chile
[10] Instituto de Ecología & Biodiversidad (IEB), Santiago, Chile
[*] Author to whom any correspondence should be addressed.

E-mail: psarricolea@uchilefau.cl

Keywords: Chile, heat vulnerability index (HVI), Iquique–Alto Hospicio, land surface temperature (LST), local climate zones (LCZs), spatial autocorrelation, surface urban heat island (SUHI)

Abstract

Heat vulnerability is a critical issue for cities under climate change, especially in socially precarious contexts and extreme climates such as deserts. The Iquique–Alto Hospicio conurbation in northern Chile represents a distinctive case study due to its marked altitudinal contrasts and rapid urban expansion. This research focuses on assessing the Surface Urban Heat Island (SUHI) at its peak expression, during summer nighttime conditions, in order to spatialize heat vulnerability. A multi-scalar workflow was applied, beginning with long-term multitemporal analysis of land surface temperature at moderate resolution (2002–2023) and extending to high-resolution downscaling for five recent years (2019–2023) using bilinear resampling combined with robust regression techniques. A heat vulnerability index was then developed through principal component analysis (four components, ∼74% variance explained), complemented by a spatial cluster analysis based on Anselin's Local Moran's I, which delineated statistically significant hot-spots in Iquique's historic core and in recently formalized social-housing districts on the Alto Hospicio plateau, as well as cold-spots along the affluent coastal seafront. The results confirm the presence of a strong nocturnal summer SUHI, largely coinciding with the most densely populated areas characterized by low-rise housing and limited green space. The local climate zone Compact low-rise and lightweight built forms were identified as the most vulnerable to heat. The study concludes that effective strategies should promote less dense building typologies while incorporating urban infrastructures that act as climate refuges across the conurbation. More broadly, the approach offers a transferable template for climate-resilient planning in data-scarce, arid coastal cities worldwide.

Acronyms

AHCs	Access to health centers
AWS	Access to water supply
DJF/MAM/JJA/SON	Seasonal climatologies (December–February, March–May, June–August, September–November)
EI	Employability index
ELI	Educational level
HQI	Housing quality index
HVI	Heat vulnerability index
INE	Instituto Nacional de Estadísticas (Chile)
LCZ	Local climate zone
LISA	Local indicators of spatial association
LST	Land surface temperature
MODIS	Moderate resolution imaging spectroradiometer
NDVI	Normalized difference vegetation index
PCA	Principal component analysis
QA	Quality assurance
RLSs	Robust least squares
R^2	Coefficient of determination
SES	Socioeconomic status
SUHI	Surface urban heat island
SUCI	Surface urban cool island
UAI	Universidad Adolfo Ibáñez

1. Introduction

Beyond global climate change, urbanization intensifies extreme heat events through land-use and land-cover changes, such as reduced vegetation and increased impervious surfaces. These transformations alter surface properties, enhance aerosol emissions and anthropogenic heat, and suppress surface winds, collectively amplifying urban warming (Sun *et al* 2018, Wu *et al* 2021). Recent studies have shown that these land-use and land-cover transformations strongly determine the spatial configuration of thermal environments, with built-up, vegetated, and bare-surface mosaics exhibiting markedly distinct surface energy responses (Fuladlu 2022). Although urbanization is a key driver of urban warming, cities with growth rates that are located in hyperarid-coastal areas can experience greater warming sensitivity due to surrounding low density forest cover and climatic conditions, making desertic climate cities particularly interesting for study (Wei *et al* 2023, Liu *et al* 2025). In this regard, the capacity of the LCZ framework to differentiate urban thermal environments across large metropolitan regions has been demonstrated in diverse contexts (e.g. China's megacities), suggesting that LCZ mapping can effectively capture morphological and radiative contrasts that underlie surface temperature variability (Zhou *et al* 2023). Contributions to the thermal environment differ among LCZs, with temperature increases of 1.1°–1.6°C during the day and 1.3°–2.2°C at night during particularly heat events. High-rise and compact building forms are the main urban elements drivers of this temperature rise (Ma *et al* 2024).

Compound (day–night) heat extremes pose great health risks, particularly for women, children and older urban residents (van Steen *et al* 2019, Limaye 2023, Zhou *et al* 2025). Such events have increased significantly since the mid 20th century, driven by urban expansion and anthropogenic emissions. Urbanization, greenhouse gases, and other factors contribute to this trend (Wang *et al* 2021). In Mediterranean and insular settings, remote sensing evidence confirms that intensified anthropogenic emissions and urban expansion jointly elevate LST and pollutant concentrations, reinforcing the coupling between human activity and thermal stress (Fuladlu 2024). Projections suggest that these events could become two to five times more frequent by the 2090s, which would significantly increase the exposure of the urban population to 83.55 billion person-days. Urbanization is expected to further amplify exposure to anthropogenic climate change-induced heatwaves from 74.79 billion to 110.9 billion person-days (Luo *et al* 2024).

SUHIs in arid cities display patterns that diverge markedly from those documented in sub-humid and humid urban environments (Haashemi *et al* 2016). In many arid and semi-arid settings, daytime urban surfaces can be cooler than the adjacent non-urban and rural lands, producing an 'oasis effect', or even an SUCI. This is because building shade and, in some cases, irrigated vegetation moderate surface temperatures relative to the surrounding bare, dry soils (Chen *et al* 2022). After sunset, however, cities typically retain more heat, and the classical SUHI manifests with higher urban temperatures than those of the outlying areas (Fan *et al* 2017, Gourfi *et al* 2022). Given that each city constitutes a unique

case, analyzing SUHI dynamics in arid contexts requires a particular assessment of both the indicators employed and their temporal resolution; critically, studies must incorporate daytime and nighttime data to inform the design of effective, context-specific mitigation strategies (Shahfahad *et al* 2023). However, the definition of rural or non-urban reference areas remains a significant source of uncertainty in SUHI quantification, as diverse delineation methods can produce large seasonal and spatial differences in measured intensities (Fu *et al* 2024).

However, this study focuses on heat as a problem not only of thermal comfort of SUHIs, but also as a health problem, emphasizing vulnerability to heat. Heat exposure of urban population is caused by both global warming due to anthropogenic climate change (Coffel *et al* 2017, Mora *et al* 2017) and by the urban heat island phenomenon (Wouters *et al* 2017, Manoli *et al* 2019), with multiple and hazardous effects on human health (Wang *et al* 2024, Yang *et al* 2024). In a study conducted for 13 115 cities from 1983 to 2016, and based on a daily maximum temperature threshold of 30 °C, global exposure rose by approximately 200% between 1983 and 2016. Total urban warming accounted for a 52% greater annual increase in exposure than urban population growth alone. Exposure trends intensified in 46% of urban areas, encompassing 23% of the global population (1.7 billion people) by 2016. Nonetheless, the relative influence of urban warming and population growth on exposure trajectories varied spatially (Tuholske *et al* 2021).

Addressing climate risks of this scale represents an unprecedented challenge for many urban areas (Georgi *et al* 2016). To address the limited understanding of adaptation processes, the concept of adaptive capacity has gained prominence in urban resilience discourse. While often included in vulnerability and resilience assessments, its standalone measurement and modeling remain underdeveloped. Despite ongoing efforts to define and quantify adaptive capacity, there is little consensus on what constitutes effective adaptation, resulting in a lack of standardized models and indicators (Craft and Fisher 2016). Adaptation strategies have very often demonstrated effectiveness when facing extreme heat events. For example, temperature extremes negatively impact short-term consumption. Long-term projections suggest climate change will reduce aggregate consumption under both moderate and severe scenarios unless adaptation occurs—under which no significant decline occurs (Lai *et al* 2022). Other adaptation strategies against extreme heat, such as the installation of targeted cool roofs in the hottest zones of urban environments, not only reduces exposure for the greatest number of people but also exemplifies how needs-based infrastructure can support equitable heat adaptation in urban areas (Broadbent *et al* 2022). But adaptive capacity does not necessarily lead to effective adaptation, particularly given the lack of consensus on what constitutes adequate adaptation and the absence of agreed-upon models and indicators for its measurement (Martín and Paneque 2022). The uneven interaction between social and ecological systems has resulted in inequitable exposure to urban heat (Sarricolea *et al* 2022). Targeted adaptation and mitigation strategies—particularly through greenspace design and management—supports heat risk reduction and sustainable urban development (Wang *et al* 2023).

The HVI is a risk-analysis tool that operationalizes the climate-vulnerability framework of the IPCC AR6, explicitly combining hazard, exposure, sensitivity and adaptive capacity in a single construct. This integrative design allows the index to be mapped across a wide range of spatial scales, from municipalities to individual urban or census blocks. One of the earliest prototypes of the HVI was developed by Reid *et al* (2009), who applied the approach to heat-wave mortality in the United States. They analyzed ten vulnerability variables and used principal-component analysis to condense them into a smaller set of factors. Although the application of such indices to climatic hazards is relatively recent, the conceptual lineage can be traced to Cutter *et al* (2003, 2010a, 2010b), who introduced composite metrics for assessing vulnerability to environmental threats. In practice, the HVI has become a strategic instrument for prioritizing urban interventions: its outputs can inform the placement of green infrastructure and nature-based solutions, guide improvements in public space and, ultimately, help save lives in an increasingly warmer climate where certain population groups are disproportionately at risk. A comprehensive search for 'heat vulnerability index' in the Web of Science (accessed 10 June 2025) retrieves more than 900 scientific articles, most of which employ land-surface temperature and the SUHI as the primary hazard variables, while commonly incorporating covariates such as NDVI, age structure, socio-economic inequities and household income. Many studies have identified regular differences in HVI under different LCZs and social resource distribution, with compact high- and mid-rise ones being more exposed to extreme heat events with high impacts on human health (Chen *et al* 2023, Ma *et al* 2023, Zhang *et al* 2023, Zou *et al* 2025). The PCA method is the most widely used to determine the HVI of a given study case (Harlan *et al* 2006, Reid *et al* 2012, Niu *et al* 2021, Garcia-Sierra and Domene 2022).

The bibliometric network derived from 935 records (1985–2025) reveals four well-defined thematic clusters that capture the state of heat-vulnerability research (figure 1). The red cluster centers on climate-ecological extremes, linking vegetation stress and modeled future scenarios; the green cluster assembles

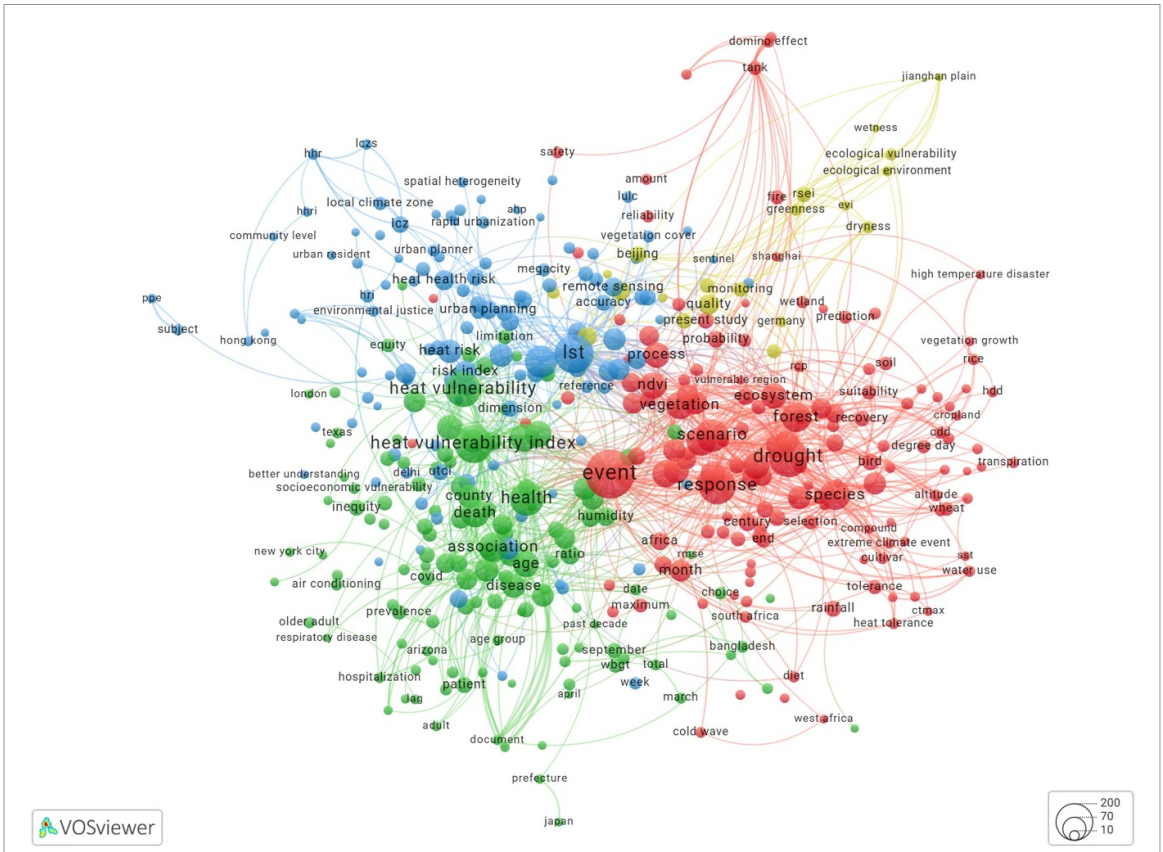

Figure 1. Co-occurrence network of terms in heat-related vulnerability research, 1985–2025. Node size represents term frequency and link thickness denotes co-occurrence strength. Four thematic clusters are evident: Red—Climate extremes, Green—Health and social vulnerability, Blue—Urban thermal remote sensing, and Yellow—Risk assessment and governance. (Interactive version: https://app.vosviewer.com/?json=https%3A%2F%2Fdrive.google.com%2Fuc%3Fid%3D17WvT8kLBrBMpyyzQJLd-EsHmnERj9dIj). The legend in the bottom-right corner indicates the number of occurrences represented by each reference circle (e.g. 10, 70, 200).

public-health evidence, dominated by the HVI and excess mortality in socio-economically disadvantaged groups; the blue cluster groups remote-sensing approaches to urban heat, with land-surface temperature, urban heat islands and LCZs as recurrent terms; the yellow cluster combines prospective risk assessment and governance, emphasizing multi-hazard vulnerability analysis and policy relevance. Bridging terms such as 'heat vulnerability', 'environmental justice' and 'vegetation cover' connect these clusters, indicating emerging interdisciplinarity yet also revealing conceptual gaps, notably the limited integration of urban inequity with satellite-derived thermal metrics and the scant linkage between drought impacts and health outcomes. These structural insights highlight opportunities for future research that integrates fine-scale remote sensing with equity-focused health assessments and adaptive urban planning, particularly in arid city contexts.

Despite recent progress, urban-climate research along Chile's hyper-arid coast remains fragmentary: case studies for Arica (Quintana-Talvac *et al* 2021, Olivares *et al.* 2025), which has also been studied using Unmanned Aerial Vehicles (Smith *et al* 2021), and Antofagasta (Palme *et al* 2019) show that SUHI intensity and socio-spatial inequalities differ sharply from patterns reported for temperate climates, yet comparable analyzes for Iquique–Alto Hospicio are virtually absent; mesoscale work using LCZ for northern Chilean cities indicates that arid coastal morphologies (low-rise canyons surrounded by bare soil) amplify nocturnal heat but provides little guidance on intra-urban mitigation strategies (Smith *et al* 2023); and emerging studies on fog harvesting in Alto Hospicio highlight the need to couple thermal stress with water scarcity but do not quantify health outcomes (Carter *et al* 2025). This knowledge gap matters because Iquique (sea-level, cooled diurnally by the Humboldt Current) and Alto Hospicio (500 m a.s.l. above the coastal cloud deck) form a steep vertical gradient where low humidity, intense solar radiation, and rapid urban expansion converge to create micro-environments of extreme perceived heat that are not captured by air-temperature records alone. Heat-index mapping—integrating temperature and moisture to express physiological stress—can therefore reveal neighborhood-scale risk hotspots, guide equitable placement of shade, vegetation and cooled refuges, and inform early-warning systems for populations with limited adaptive capacity in one of the driest urban corridors on Earth.

The main objective of this study is to identify which neighborhoods in the Iquique–Alto Hospicio conurbation are most vulnerable to heat. To this end, we first analyze 20 years of MODIS LST (2002–2023) to characterize seasonal and diurnal patterns of the SUHI. To capture intra-urban thermal gradients, summer nighttime MODIS data are downscaled to 10 m resolution using Sentinel-2 reflectance (2019–2023). Heat vulnerability is then quantified through a multidimensional HVI, constructed via PCA of demographic, socioeconomic, infrastructural, and environmental indicators. To assess spatial dependence, we apply Anselin Local Moran's I, which identifies statistically significant clusters of high and low vulnerability. Finally, the HVI is linked to the LCZ framework, enabling us to examine how urban morphology modulates the relationship between thermal exposure and socio-spatial vulnerability. This multi-scale workflow provides an integrated basis for understanding and mitigating heat risk in hyper-arid coastal cities. Building on this framework, the study addresses the following research question: To what extent do urban morphology (LCZ types) and socio-demographic factors interact to explain neighborhood-level differences in heat vulnerability, and where are the statistically significant hotspots located?. The article is organized as follows: section 2 details data sources and methods, including SUHI detection, multiresolution downscaling, HVI construction and LCZ mapping; section 3 presents the spatiotemporal SUHI patterns, high-resolution LST maps, and the spatial correspondence between HVI and LCZ typologies; section 4 discusses the implications of these findings for urban-climate theory and planning in hyper-arid coastal settings, critically assesses methodological limitations and data uncertainties, outlines the study's scope, and synthesizes the main conclusions while proposing avenues for mitigating heat exposure and refining future research.

2. Study area and methods

2.1. Study area

This study is set within the urban conurbation of Iquique and Alto Hospicio (20°12′51″S, 70°09′09″W), two municipalities in the province of Iquique, located in the Tarapacá Region of northern Chile. Iquique and Alto Hospicio constitute Chile's second-largest hyper-arid conurbation by population. Influenced by a cold semi-arid climate (BSk) and cold arid climate (BWk) (Sarricolea *et al* 2017) with mean annual precipitation under 2 mm in the last 30 years (being the city with the lowest rainfall in South America) and 17.2 °C mean annual temperature. Its unique topography and abrupt urban transitions make it an ideal case for SUHI analysis, because Iquique is situated on the Coastal Plain of the Atacama Desert, whereas Alto Hospicio lies on the elevated platform of the Coastal Range above 500–600 m a.s.l. (figure 2).

According to the 2017 Census, the municipality of Iquique had 202 891 inhabitants, with 98.34% residing in urban areas, while in Alto Hospicio the population was 113 098, where 97.98% of its inhabitants correspond to urban areas. According to INE projections, in 2025 the population of Iquique will be 233 228 inhabitants, showing an increase of 14.95%. On the other hand, Alto Hospicio projects 146 337 inhabitants, which translates into an increase of 29.38% of its population, which is high in comparison with Chile, with 9.7%.

As mentioned above, this research is situated within the cities of Iquique and Alto Hospicio, which together form a continuous urban area known as a conurbation. Consequently, satellite imagery used for the development of LCZs, as well as the HVI, was processed at the urban scale. While LCZs were constructed independently for each city at their respective urban scales, all remaining analyzes were conducted using the conurbation's unified urban scale.

2.2. Identification of daytime- vs. nighttime-dominated SUHI with MODIS

Daily LST scenes from MODIS-Terra (MOD11A1 v6.1) and MODIS-Aqua (MYD11A1 v6.1) were retrieved and processed in Google Earth Engine for the 22 year period 2002–2023. MODIS was selected because it provides the longest continuous daily LST record (since 2000) with global coverage, a proven reliability in arid environments, and standardized quality-control layers that allow robust multi-decadal analysis. Pixels were retained only when the internal QA flags recorded 'good' or 'average' retrievals (bits 0–1), radiometric values were converted from Kelvin to degrees Celsius using:

$$\text{LST } °C = (\text{LST digital number} \times 0.02)—273.15.$$

Cloud/cirrus and poor-geometry pixels were excluded using the MODIS QA layers. To enhance spatial detail while limiting artifacts, each 1 km image was bilinearly resampled to 500 m and then to 250 m, following the scale-refinement approach of Liu and Weng (2018) and Sarricolea *et al* (2022). The remaining cloud-free and quality-controlled daily imagery was composited into climatological seasons:

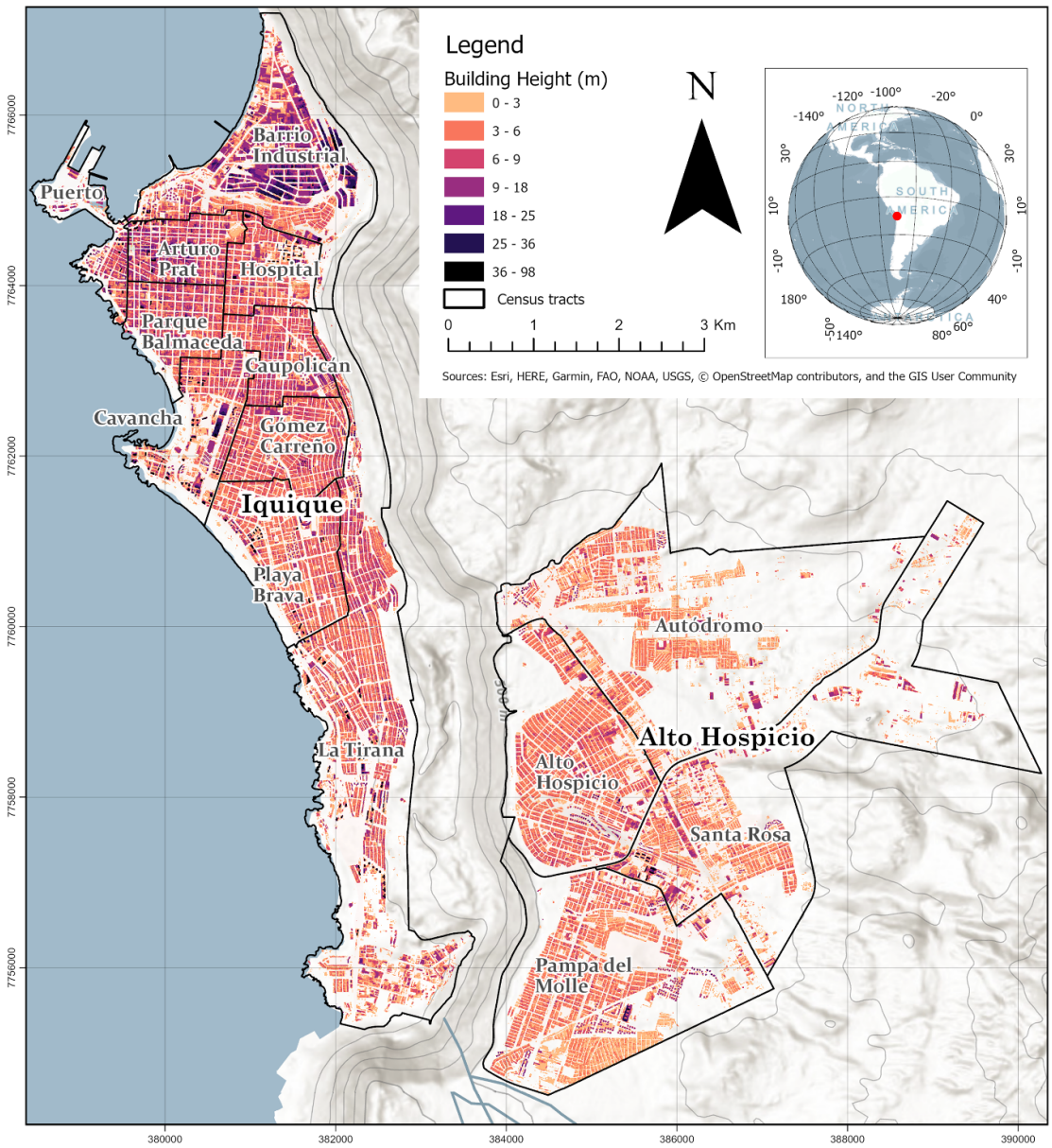

Figure 2. Study area showing also the different building heights. Building height data from Open Buildings 2.5D temporal dataset, available on Google earth engine.

DJF (summer), MAM (autumn), JJA (winter) and SON (spring), for every year, yielding 88 seasonal rasters per satellite mission.

Because the conurbation straddles $a > 500$ m escarpment, two separate rural references were defined. The coastal plain surrounding Iquique (ranging between 0 m and approximately 50 m a.s.l.) served as the low-elevation rural mask, whereas sparsely vegetated surfaces on the plateau east of Alto Hospicio (from about 500–600 m a.s.l.) formed an independent high-elevation rural mask. This distinction removes the lapse-rate bias that would arise if a single rural baseline were applied across the altitude gradient, ensuring that urban–rural temperature differences isolate the effect of land-cover change rather than topography.

2.3. Robust-regression downscaling of summer-night LST to 10 m with Sentinel-2

To resolve the fine-scale thermal mosaic of the conurbation we adapted the Daily Ten-ST-GEE workflow of Mhawej and Abunnasr (2022). A total of 137 MODIS summer-night scenes (2019–2023) were paired with cloud-free Sentinel-2 Level-2 A imagery (COPERNICUS/S2_SR_HARMONIZED); rigorous cloud masking yielded 72 valid pairs. MODIS LST (already resampled to 250 m) and Sentinel-2 bands (10 m) were co-registered on a common UTM grid. The predictive stack combined Sentinel-2 bands B2–B4, B8, B11, B12 with the indices. For each date a RLSs regression related MODIS LST to the predictor stack.

RLS was chosen over Ordinary Least Squares and other machine-learning alternatives because it is resistant to outliers, does not rely on strict distributional assumptions, and iteratively reweights residuals using the Talwar cost function. This allows the model to capture the non-linear and heterogeneous land-surface relationships between coarse MODIS LST and fine-resolution Sentinel-2 predictors with reduced bias and lower mean absolute error, as shown in Mhawej and Abunnasr (2022).

The performance of the RLS regression was further evaluated by computing the root mean square error (RMSE) of residuals between MODIS LST and downscaled estimates. Our models yielded RMSE of approximately 0.60–0.97 °C, which are well within the range reported by Mhawej and Abunnasr (2022). These values confirm that our downscaling procedure achieves comparable accuracy and reliably resolves fine-scale nocturnal LST heterogeneity.

This approach allows for substantial spatial sharpening of LST patterns and provides detailed daily LST fields suitable for analysis and thermal vulnerability mapping.

2.4. HVI construction

The HVI was constructed following a multidimensional framework that integrates exposure, sensitivity, and adaptive capacity, adjusting established approaches from recent literature (Reid *et al* 2009, Johnson *et al* 2012, Maier *et al* 2014). Exposure indicators include LST and population density. Sensitivity covers demographic factors such as age, gender, and educational/employment conditions, reflecting social susceptibility to heat. Adaptive capacity encompasses material and infrastructural resources, environmental conditions, and access to services that enable communities to reduce, cope with, or recover from heat impacts. SES was included as a core adaptive capacity variable, as higher SES enables access to adaptive resources (e.g. better housing, health care, technology, and green spaces), reducing vulnerability to heat. Depending on the statistical distribution of each indicator, we applied (i) percentile-based min–max scaling between the 5th and 95th percentiles (P5–P95) for nearly symmetric or mildly skewed variables, (ii) a log-transformation followed by the same P5–P95 min–max rescaling for strongly right-skewed variables (e.g. population density, AWS), and (iii) an ordered-category rescaling to the 0–1 interval for the socioeconomic-status index (see table 1). After rescaling, directionality was harmonized so that higher values of adaptive-capacity indicators decrease overall vulnerability. All computations were first performed at the census block level, the finest unit available in Chile, and then aggregated to the census tract level for analysis and interpretation. This dual-scale approach ensures maximum spatial detail while maintaining compatibility with official socio-demographic reporting.

2.5. PCA for variable reduction

To reduce the dimensionality of socio-environmental indicators and avoid multicollinearity, a PCA was performed using R language (version 4.5.0). All input variables were standardized (centered and scaled to unit variance) prior to analysis to ensure comparability. The PCA was implemented using the prcomp() function, and an orthogonal Varimax rotation was subsequently applied with the varimax function to improve the interpretability of the resulting components. The Varimax rotation is commonly used in environmental and social sciences because it maximizes the variance of squared loadings within each component, resulting in a clearer association between variables and components. Prior to PCA, we examined collinearity using correlation matrices and identified two pairs of variables with high correlations above 0.8: Female population with Population density ($r = 0.91$) and ELI with SES ($r = 0.88$). We nevertheless retained the full set of 12 indicators, since each captures a distinct conceptual dimension of heat vulnerability. PCA inherently mitigates multicollinearity by generating orthogonal components, and sensitivity checks confirmed that the component structure remained stable when highly correlated variables were excluded.

The number of principal components to retain was determined by the Kaiser criterion (Kaiser 1960), which recommends keeping components with eigenvalues greater than one. Four components were retained, together explaining ∼74% of the variance (table 2). Component z-scores were summed to create the composite HVI (Reid *et al* 2009).

Each of the four retained principal components was standardized using z-scores (mean = 0, standard deviation = 1) prior to aggregation. The final HVI was calculated as the sum of the z-score values for each component, a common practice in the construction of composite indices (Reid *et al* 2009). This method preserves the relative contributions and directionality of each principal component.

As a result, the HVI values for the study area range approximately from −5 to 6, reflecting the combined distribution of the standardized components. These values are interpreted on a relative scale, where higher index values indicate greater vulnerability to heat. If required for ease of interpretation or comparison with other indices, the composite HVI can be further normalized using min–max scaling (to a 0–1 range) or re-standardized as a z-score.

Table 1. Indicators, data sources, normalization, directionality, and references used to construct the HVI for Iquique–Alto Hospicio, Chile.

Dimension	Indicator	Calculation of variables by census blocks	Data source	Observed Distribution	Normalization Method/ Directionality	Supporting references	Justification
Exposure	LST	Mean pixel values by 10 m	MODIS and SENTINEL-2 (Daily Ten-ST-GEE, 2019–2023)	Slight skewness, some outliers	Min–max percentile (P5–P95)/Positive	Johnson *et al* (2012); Niu *et al* (2021); Inostroza *et al* (2016)	LST is a primary indicator of thermal exposure and widely used in HVIs to represent urban heat hazard.
	Population density	Number of people per hectare	Population and Housing Census 2017 (INE)	Highly skewed	Log + min–max percentile (P5–P95)/Positive	Tuholske *et al* (2021); Manoli *et al* (2019)	Population concentration directly increases exposure to heat extremes and urban SUHI intensity.
Sensitivity	Elderly population	Number of older adults aged 65 years or more per hectare	Population and Housing Census 2017 (INE)	Skewed, mostly low values	Min-max percentile (P5–P95)/Positive	Reid *et al* (2009); van Steen *et al* (2019)	Older adults are consistently identified as highly vulnerable to heat-related morbidity and mortality.
	Infant population	Number of infants 5 years old or younger per hectare	Population and Housing Census 2017 (INE)	Highly skewed, long tail	Min–max percentile (P5–P95)/Positive	Johnson *et al* (2012); Reid *et al* (2012)	Infants are more sensitive to heat due to lower thermoregulation capacity.
	Female population	Number of women per hectare	Population and Housing Census 2017 (INE)	Skewed, some isolated high values	Min–max percentile (P5–P95)/Positive	van Steen *et al* (2019); Limaye (2023)	Women, especially elderly, show higher heat-related mortality risks in epidemiological studies.

(Continued.)

Table 1. (Continued.)

	Educational level (ELI)	Zonal mean of the average years of education of household heads	Territorial Human Well-being Matrix 2021 (UAI) available at https://matrizbht.cl/	Slight skewness	Min–max percentile (P5–P95)/Negative	Reid *et al* (2009, 2012); Inostroza *et al* (2016); Olivares *et al* (2025)	Low education is linked to reduced adaptive capacity and higher heat vulnerability.
	Employability (EI)	Zonal mean of the proportion of the labor force with employment	Territorial Human Well-being Matrix 2021 (UAI) available at https://matrizbht.cl/	Slightly skewed	Min–max percentile (P5–P95)/Negative	Johnson *et al* (2012); Garcia-Sierra and Domene (2022)	Unemployment or low employability indicates socioeconomic disadvantage, reducing adaptive capacity.
Adaptive capacity	Housing quality (HQI)	Zonal mean of all materials per household (walls, floors, ceilings)	Territorial Human Well-being Matrix 2021 (UAI) available at https://matrizbht.cl/	Accumulated at the upper end	Min–max percentile (P5–P95)/Negative	Harlan *et al* (2006); Reid *et al* (2012)	Poor housing quality increases indoor heat stress, especially in low-income neighborhoods.
	Access to water supply (AWS)	Number of households with access to the public water network per hectare	Population and Housing Census 2017 (INE)	Highly skewed	Log + min–max percentile (P5–P95)/Negative	Inostroza *et al* (2016); Carter *et al* (2025)	In arid cities, lack of access to water aggravates vulnerability by limiting hydration and cooling.
	Access to health centers (AHC)	Zonal mean of public and private health centers per inhabitant	Territorial Human Well-being Matrix 2021 (UAI) available at https://matrizbht.cl/	Moderate skewness	Min–max percentile (P5–P95)/Negative	Romero-Lankao *et al* (2012); Georgi *et al* (2016); Martín and Paneque (2022;)	Access to health services is critical to adaptive capacity and rapid response during heat events.
	NDVI	Mean pixel values by 10 m	SENTINEL-2, MSI, 2019–2023	Slight skewness	Min–max percentile (P5–P95)/Negative	Johnson *et al* (2012); Reid *et al* (2012); Inostroza *et al* (2016)	Vegetation reduces surface temperature and mitigates urban heat exposure.
	SES (Socioeconomic status)	Socioeconomic status index (ordered categories; higher values = higher SES)	Entel-Ocean 2023	Stepped/categorical	Min–max percentile (P5–P95), categories ordered by SES	Harlan *et al* (2006); Sarricolea *et al* (2022)	Low SES is strongly linked to higher heat vulnerability due to limited adaptive resources.

Note: The table summarizes the indicators used to construct the multidimensional HVI following the framework of exposure, sensitivity, and adaptive capacity. Directionality was standardized so that higher values of adaptive-capacity variables indicate lower vulnerability (negative direction).

Table 2. Eigenvalues, variance explained, and proportion for retained principal components following PCA with Varimax rotation.

Principal component	Eigenvalue	Proportion of total variance	Percentage of explained variance
Component 1	3.72	0.3099	30.99%
Component 2	2.69	0.2242	22.42%
Component 3	1.51	0.1258	12.58%
Component 4	0.96	0.0798	7.98%

Note: Only components with eigenvalues greater than 1 were retained according to the Kaiser criterion. The cumulative variance explained by these four components accounted for approximately 74% of the total variance.

To reveal statistically significant clusters and outliers of heat vulnerability at the 95% confidence level ($p < 0.05$), we ran an Anselin Local Moran's I cluster–outlier analysis in ArcGIS Pro 3.3 on the census block layer, using the composite HVI as the input variable. Spatial relationships were conceptualized with an inverse-distance weighting scheme based on Euclidean distance, and row standardization was applied so that each tract contributed equally to the statistic. A fixed 800 m distance band, identified from the peak in incremental spatial autocorrelation, defined each feature's neighborhood. This threshold (800 m) was also consistent with the average size of census tracts in the study area, ensuring that hot- and cold-spot clusters were detected at a scale directly interpretable for census-based vulnerability analysis. Statistical significance was evaluated with 199 Monte-Carlo permutations, and a false discovery rate (FDR) correction was applied to control for multiple comparisons; only tracts with FDR-adjusted p-values $\leqslant 0.05$ were retained as significant. The resulting feature class classified tracts into high–high clusters, low–low clusters, high–low outliers, low–high outliers, non-significant areas, and features with no neighbors, following Anselin's original formulation of Local Moran's I (Anselin 1995).

2.6. LCZs

LCZs were derived following Stewart and Oke (2012) by classifying urban morphology according to surface structure and materiality. The 2023 dataset, supplied by Smith *et al* (2023), is mapped in figure 3. Every urban block and its surrounding area were delineated with the standard LCZ framework, which recognizes ten built-form categories (LCZ 1–10) and seven land-cover categories (LCZ A–G), each defined by characteristic building shapes, surface types, vegetation, and dominant construction materials. Field inspection and high-resolution imagery confirmed that several standard classes are absent from the hyper-arid, steep-sloped study area: sparsely built zones (LCZ 9), densely or scattered wooded areas (LCZ A–B), and open-water bodies (LCZ G) do not occur within the mapped extent. Instead, the landscape is dominated by compact and open built forms (LCZ 1–8, 10) together with shrub/scrub (LCZ C), low plants (LCZ D), extensive paved or rocky ground (LCZ E), and bare soil or sand (LCZ F). In Alto Hospicio—particularly in neighborhoods such as Pampa del Molle—many residential clusters originated as informal *campamentos* that typically fall under Lightweight Low-rise (LCZ 7). These areas have been progressively formalized through social-housing programs, altering their urban fabric and transitioning from Lightweight Low-rise (LCZ 7) to Compact Low-rise (LCZ 3). Building on this LCZ classification, quantifies the share of each built-form zone that falls into every HVI level; the results analyze these distributions to uncover how urban morphology conditions thermal vulnerability across the conurbation.

All methodological steps described in sections 2.2–2.6 are summarized schematically in figure 4. The workflow integrates multi-temporal MODIS processing, Sentinel-2–based downscaling, indicator normalization, PCA/Varimax component extraction, HVI mapping, spatial cluster analysis (Local Moran's I), and the final HVI–LCZ cross-tabulation, providing a concise visual synthesis of the full analytical framework applied in this study.

3. Results

3.1. Spatiotemporal SUHI patterns *(MODIS 2002-2023)*

The daytime thermal mosaics (figure 5) reveal a pronounced duality between the two urban nuclei. Coastal Iquique frequently displays a positive SUHI in summer, autumn and spring, with anomalies of 0.2 °C to more than 2 °C, whereas plateau-top Alto Hospicio almost always registers a SUCI, with daytime deficits between—2 °C and below—4 °C; only the still-undeveloped eastern tract departs from this tendency, occasionally reaching values near 1 °C. During winter the coastal SUHI in Iquique vanishes, yielding near-neutral or mildly negative anomalies (–0.2 °C to—2 °C) that coincide with the season's strongest plateau cooling and accentuate the urban–periphery contrast. Night-time patterns (figure 6) are markedly different: a robust SUHI envelops both cities year-round, with the highest intensities (≈ 2 °C)

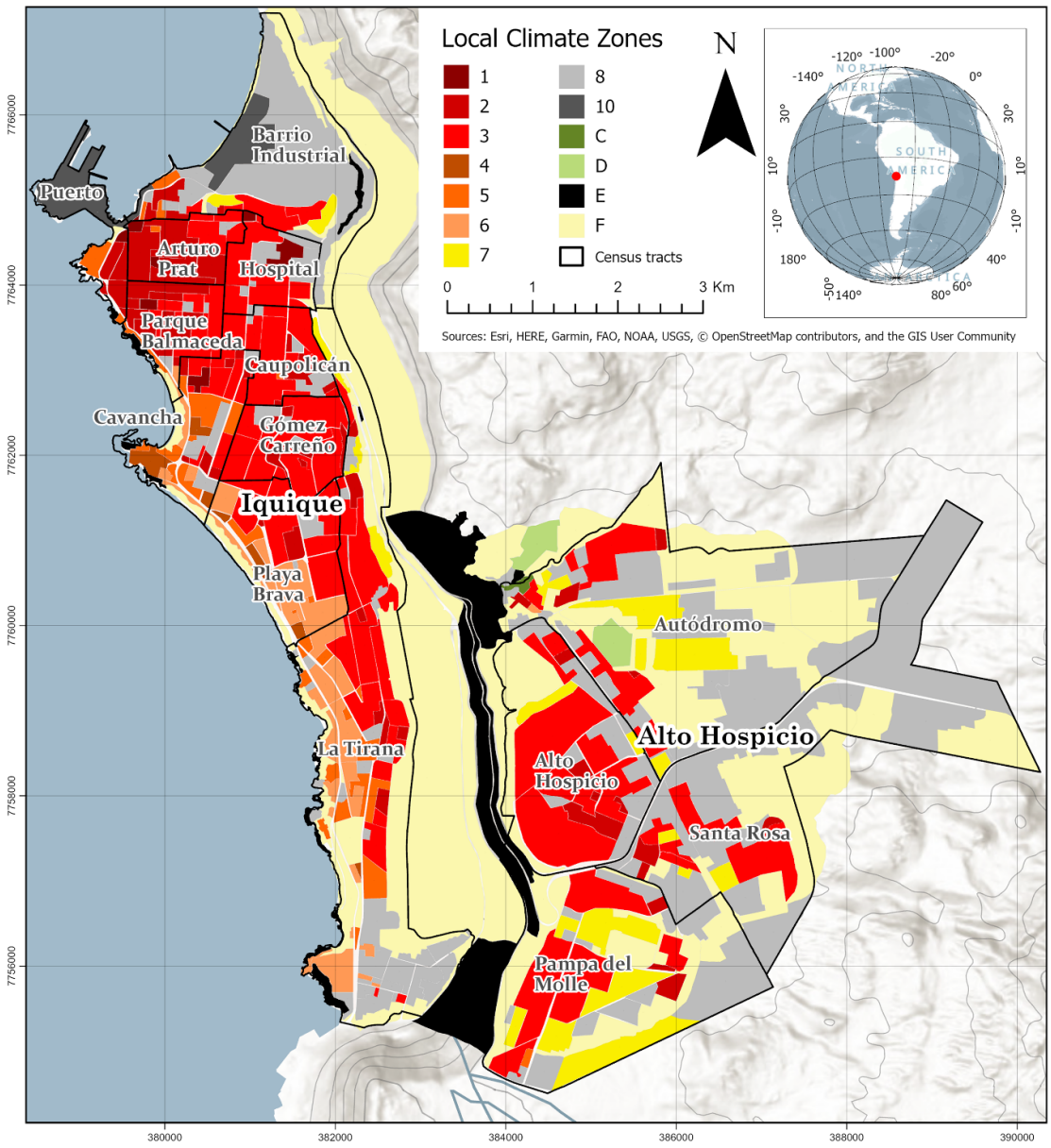

Figure 3. Local climate zone map of the Iquique–Alto Hospicio conurbation (northern Chile).

concentrated in southwestern Iquique and the lowest values (–0.5 °C to—1 °C) on the periphery of the Santa Rosa tract. In Alto Hospicio, MODIS data from 2002 to 2023 show that night-time maxima consistently occur in Pampa del Molle and minima again in Santa Rosa. During summer, for example, the average SUHI intensity ranges from—1.0 °C to 1.9 °C in Autódromo (figure 6),—1.2 °C to 1.8 °C in Santa Rosa, 1.4 °C to 2.2 °C across Alto Hospicio, and 0.2 °C to 2.3 °C in Pampa del Molle. This spatial hierarchy persists across all seasons, confirming a persistent urban–periphery thermal gradient and justifying our focus on nocturnal conditions when assessing exposure.

3.2. Downscaled nighttime LST and validation

At 10 m spatial resolution, individual streets and urban blocks are clearly delineated, and pixel-wise comparisons with MODIS nighttime LST show strong agreement, with robust R^2 values exceeding 0.65 ($p < 0.05$) and mean absolute errors below 0.5 °C. The analysis of mean nighttime LST during the summer months for the period 2019–2023 reveals a distinct spatial gradient across Iquique and Alto Hospicio, with values ranging from 15 °C to 22.6 °C (figure 7). The lowest temperatures, between 15 °C and 16.5 °C, are predominantly found on the periphery of Alto Hospicio, specifically within the census tracts of Santa Rosa and Autódromo. These cooler areas, characterized by lower building density and greater exposure to bare soils, appear as extensive blue-toned zones in the mapped results. While some isolated pockets with similar values occur at the northern edge of Iquique (Barrio Industrial), these are

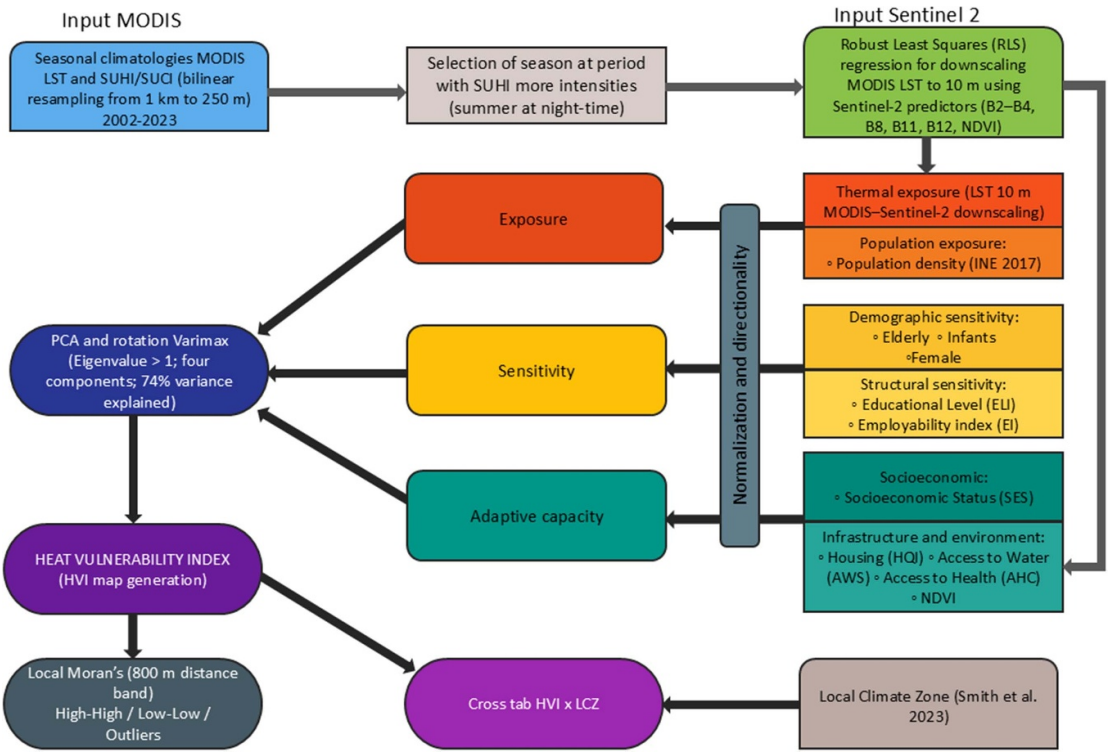

Figure 4. Methodological workflow for heat-vulnerability mapping in Iquique–Alto Hospicio.

not representative of the general conditions within any census tract. Intermediate LST values, between 16.5 °C and 18 °C, are distributed across much of Iquique, but are especially prevalent and spatially uniform throughout the urban sectors of Alto Hospicio, including the Alto Hospicio, Autódromo, and Santa Rosa census tracts. In Iquique, such temperatures also appear concentrated at the northern and southern extremes, corresponding to the Barrio Industrial and La Tirana tracts, respectively. This pattern suggests the influence of transitional urban morphologies, with moderate density and mixed land covers. In contrast, high nighttime surface temperatures, ranging from 18 °C to 22.5 °C, are widespread across Iquique's urbanized core. Maximum values are observed in La Tirana (22.6 °C) and Cavancha (22.4 °C), with the latter district notable for its concentration of high-rise buildings and dense built environment. On average, the census tracts of Hospital, Caupolicán, and Cavancha present the highest nighttime LSTs, reflecting the impact of impervious surfaces and urban form on heat retention. In Alto Hospicio, higher temperatures are also identified within the Pampa del Molle census tract, where LSTs fluctuate between 15.9 °C and 20.1 °C.

These spatial patterns are consistent with the summary statistics presented in table 3, which indicate that the most densely urbanized and built-up districts in central Iquique exhibit the highest mean nighttime surface temperatures, while the peripheral and less developed areas of Alto Hospicio remain significantly cooler. The observed urban–periphery gradient in LST highlights the interplay between urban morphology, land cover, and the intensity of the nocturnal urban heat island, suggesting implications for local microclimates and potential socio-environmental vulnerabilities.

3.3. Heat-vulnerability PCA and index distribution

The heat-vulnerability analysis used a PCA with Varimax rotation that retained four components whose eigenvalues exceeded one and together explained about 74% of the total variance (table 4). PC1 ('Urban Socio-Demographic Vulnerability') is defined by high population density, greater proportions of women, children, and older adults, and reduced AWS. This component highlights neighborhoods where both exposure and social sensitivity converge, alongside limited adaptive capacity, indicating a higher risk of adverse heat-related impacts. PC2 ('Socioeconomic Adaptive Capacity') groups together areas with higher SES, improved housing conditions, and greater educational attainment. These characteristics are associated with greater adaptive capacity, suggesting that these neighborhoods are better equipped to mitigate the negative effects of heat exposure. PC3 ('Thermal Exposure and Structural Sensitivity') loads most strongly on high LST and the presence of older adults, with an inverse association with AHCs. This

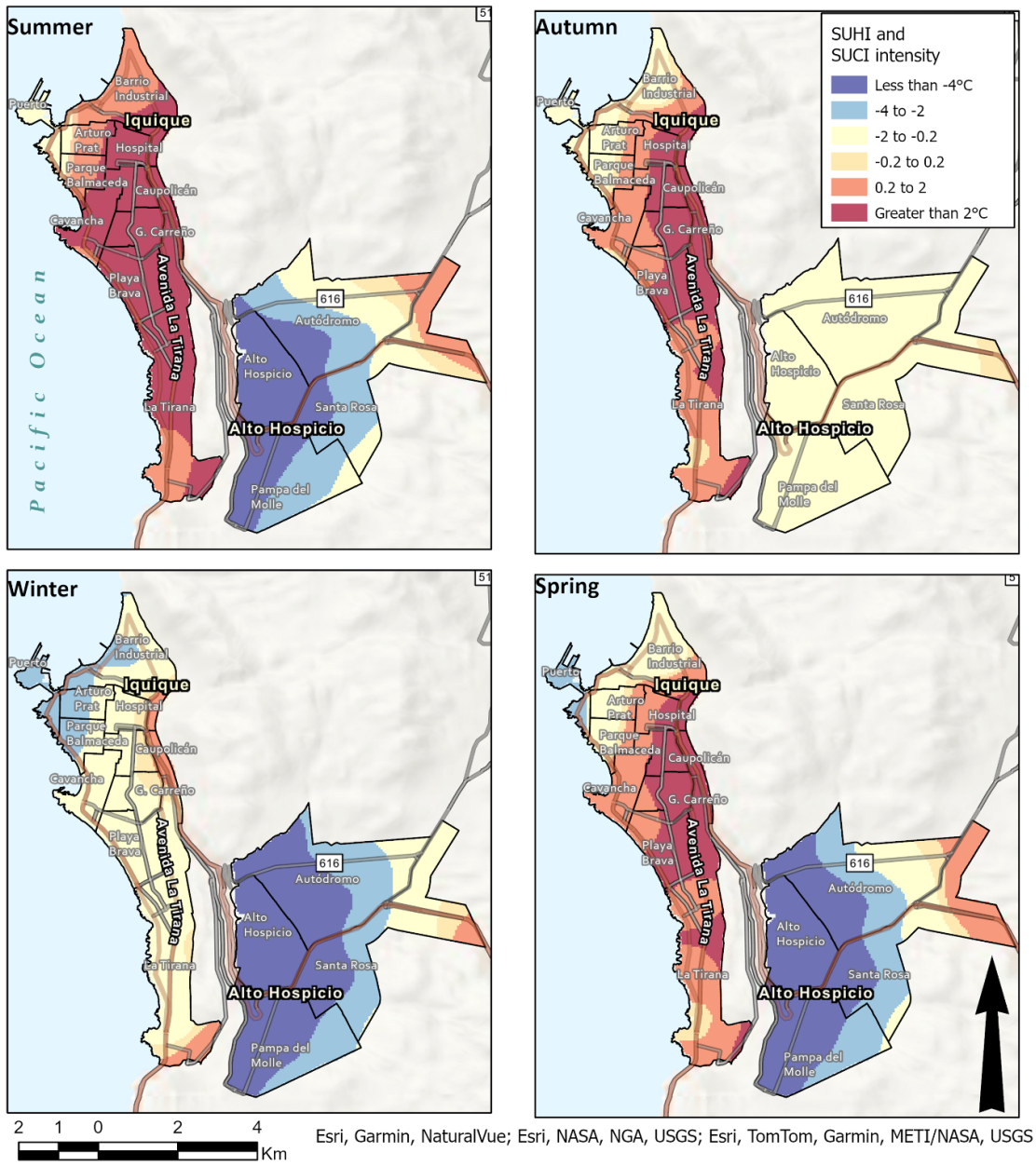

Figure 5. Spatial distribution of daytime SUHI and SUCI intensities in Iquique–Alto Hospicio during the summer season (2002–2023).

component identifies neighborhoods where physical and demographic exposure is aggravated by inadequate access to healthcare infrastructure. PC4 ('Human Capital and Reduced Sensitivity') is driven by high values of employability and ELI, which are associated with reduced social sensitivity according to the directionality defined in the conceptual framework. Neighborhoods scoring high on this component are expected to be more resilient due to the greater resources available through human capital. These four components together provide a comprehensive and multidimensional profile of urban heat vulnerability, integrating demographic, socioeconomic, environmental, and infrastructural factors.

The biplot (figure 8) displays the Varimax-rotated principal-component space constructed from the twelve standardized indicators in table 1. Component 1, runs from tracts with high demographic density and a child-rich, female-skewed population (large negative loadings for Population density, Female population and Infant population) to tracts with abundant urban services (positive loadings for AHCs, and AWS). Component 2, contrasts thermal exposure and ageing (positive loadings for LST and Elderly population) with low socio-economic status and limited housing quality (negative loadings for SES, ELI, Employability and HQI). The longest vectors belong to LST, AWS and SES, indicating their dominant

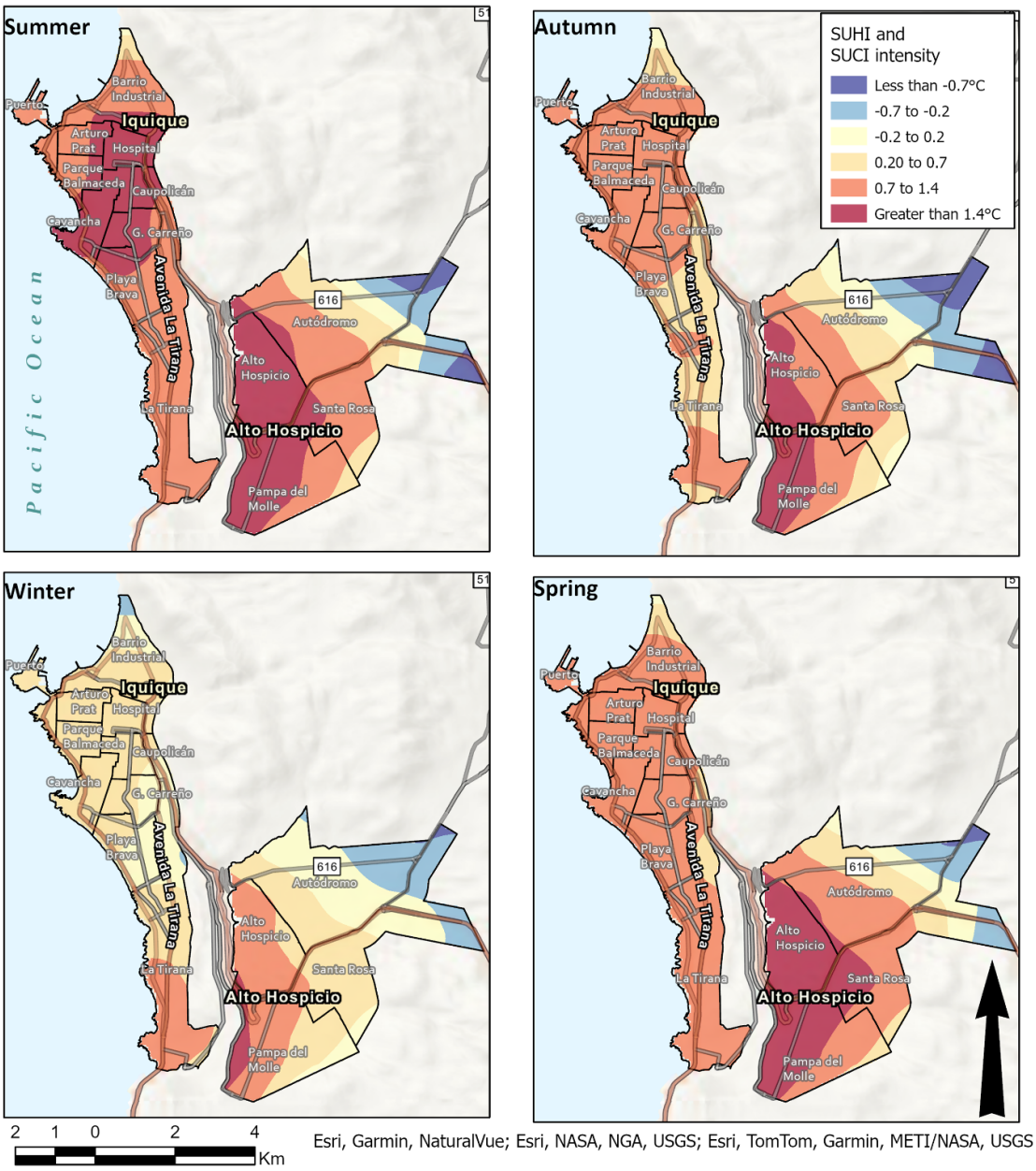

Figure 6. Spatial distribution of nighttime SUHI and SUCI intensities in Iquique–Alto Hospicio during the summer season (2002–2023).

structuring role, while the near overlap of Population density and Female population reveals a strong positive correlation. Applying k-means to the scores of these two components produces four clusters: cluster 1 (orange) represents the dense, hot urban core with ample services; cluster 2 (green) groups socio-economically disadvantaged areas with poor housing conditions; cluster 3 (blue) contains highly populated, younger districts under intermediate heat; cluster 4 (red) corresponds to service-rich zones that experience moderate nighttime temperatures. The scatter shows that intense surface heat does not always align with greater social vulnerability, highlighting the need for adaptation strategies that integrate exposure, demographic sensitivity and adaptive capacity.

Figure 9 synthesizes the standardized scores of the four principal components that make up the HVI for the Iquique and Alto Hospicio conurbation at census block scale. High socio-demographic vulnerability (Component 1) groups along Iquique's mature coastal core, from Puerto and Barrio Industrial in the north to Playa Brava in the south, where tracts contain larger shares of older adults, children, and female-headed households, while nearly the entire Alto Hospicio (including Autódromo and Pampa del Molle) records very low scores, revealing a steep coast-to-plateau gradient in social stress. The pattern

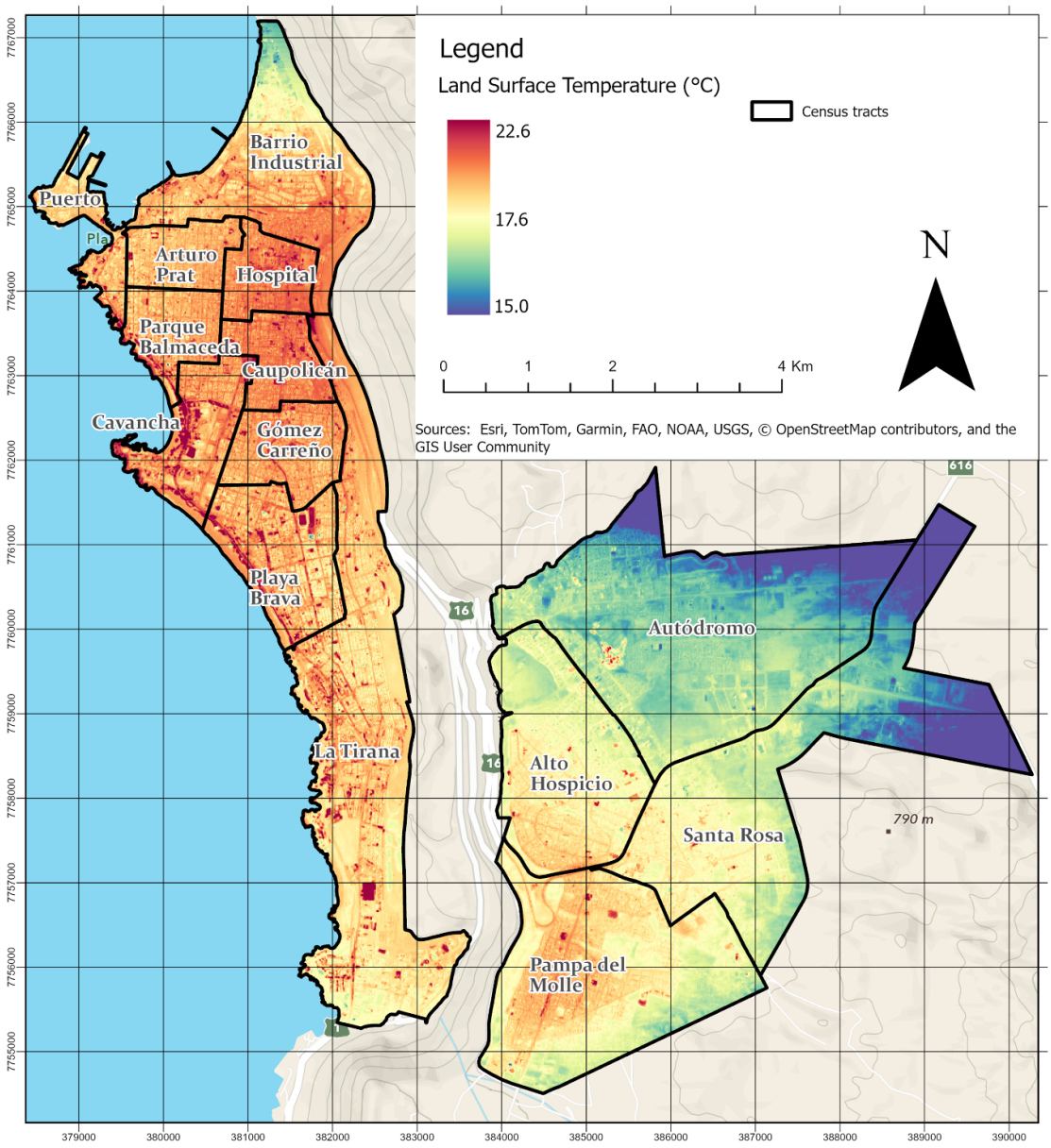

Figure 7. Nighttime summer LST in the Iquique–Alto Hospicio conurbation between 2019 and 2023.

reverses for socio-economic adaptive capacity (Component 2): very high scores appear in recently urbanized tracts east of the city and in a few affluent beachfront areas at Cavancha and Playa Brava, whereas the historic center of Iquique and the northern industrial waterfront show very low to low values, signaling limited income, poor housing quality, and scarce assets. Thermal exposure combined with health-service accessibility (Component 3) peaks in the northern industrial (ZOFRI), harbor zone, and densely built coastal strip, where elevated nighttime land-surface temperatures coincide with longer travel times to tertiary hospitals; plateau tracts in Alto Hospicio, including Santa Rosa and Pampa del Molle, display low or very low scores, reflecting cooler conditions and shorter travel distances to the regional hospital. Human capital and reduced sensitivity (Component 4) concentrate along the commercial–administrative spine of central Iquique (around Arturo Prat Avenue and Parque Balmaceda) and in selected upper-income enclaves near Autódromo, whereas most Alto Hospicio tracts fall into the medium-low category, indicating deficits in tertiary-education attainment that may offset other adaptive advantages identified in Component 2. Altogether, the maps reveal sharp coastal–inland and north–south contrasts, with pronounced intra-urban heterogeneity: coastal Iquique combines high socio-demographic vulnerability and extreme thermal exposure with comparatively low adaptive capacity, while the Alto Hospicio plateau shows the opposite profile—greater adaptive capacity but reduced human capital—underscoring the need for spatially differentiated heat-risk interventions within the conurbation.

Table 3. Nighttime summer LST by Census Tract, Iquique–Alto Hospicio (2019–2023, MODIS derived LST and resample with Sentinel-2).

Municipality	Census Tract	Min–Max (°C)	Mean (°C)
Iquique	Puerto	16.9–20.7	18.0
	Barrio Industrial	15.9–19.8	17.9
	Hospital	17.0–20.2	18.3
	Caupolicán	16.9–20.1	18.3
	Playa Brava	16.5–21.9	18.1
	Cavancha	17.0–22.4	18.3
	Parque Balmaceda	15.9–21.6	18.1
	Arturo Prat	17.2–20.1	18.0
	Gomez Carreño	17.2–20.1	18.2
	La Tirana	16.5–22.6	17.9
Alto Hospicio	Autódromo	15.5–19.2	16.8
	Santa Rosa	15.0–19.5	16.9
	Alto Hospicio	16.0–20.1	17.5
	Pampa del Molle	15.9–20.1	17.6

Table 4. PC description of each of the different components identified.

Principal component	Main loadings	Interpretation	Suggested name
PC1	Pop. density (+), Female (+), Infant (+), Elderly (+), Water Access (−)	High demographic pressure and sensitive age groups together with limited access to the water network	Urban Socio-Demographic Vulnerability
PC2	SES (+), HQI (+), ELI (+)	High socio-economic status, good housing conditions and education that underpin greater adaptive capacity	Socioeconomic Adaptive Capacity
PC3	LST (+), Elderly (+), AHC (–)	High thermal exposure and an ageing population aggravated by limited healthcare provision	Thermal Exposure and Structural Sensitivity
PC4	ELI (+), EI (+)	Elevated human capital that lowers social sensitivity to heat stress	Human Capital and Reduced Sensitivity

Following the extraction of the four varimax-rotated components, we produced the final map of the HVI using summer land-surface temperature data from 2019 to 2023. Figure 10 reveals a pronounced coastal-to-inland gradient. Most coastal tracts of Iquique—including Puerto, Cavancha and Playa Brava—fall in the Very Low or Low classes, reflecting both the maritime cooling influence and the high adaptive capacity associated with elevated socio-economic status, service provision and green-space availability. Vulnerability increases sharply inland: the urban core bounded by Arturo Prat, Hospital and Caupolicán displays a mosaic of Medium-High to Very High HVI values, indicating the combined effect of dense built fabric and heightened socio-demographic sensitivity; this sector constitutes the most vulnerable area within Iquique. The Barrio Industrial tract attains medium values despite its coastal position, probably owing to its sparse residential population and the extensive impervious surfaces of the Zofri industrial zone. On the plateau, Alto Hospicio exhibits a contrasting pattern. Santa Rosa and Autódromo show mainly low or medium–low vulnerability, consistent with the lower surface temperatures detected there, whereas central Alto Hospicio and Pampa del Molle concentrate Medium-High to Very High classes, signaling limited adaptive capacity and higher population sensitivity. Many of these tracts originated as informal settlements that later became highly compact social-housing districts. Grey polygons correspond to areas without 2017 census data, mostly large industrial parcels or undeveloped land. Overall, figure 10 highlights that the most critical zones align with dense residential corridors

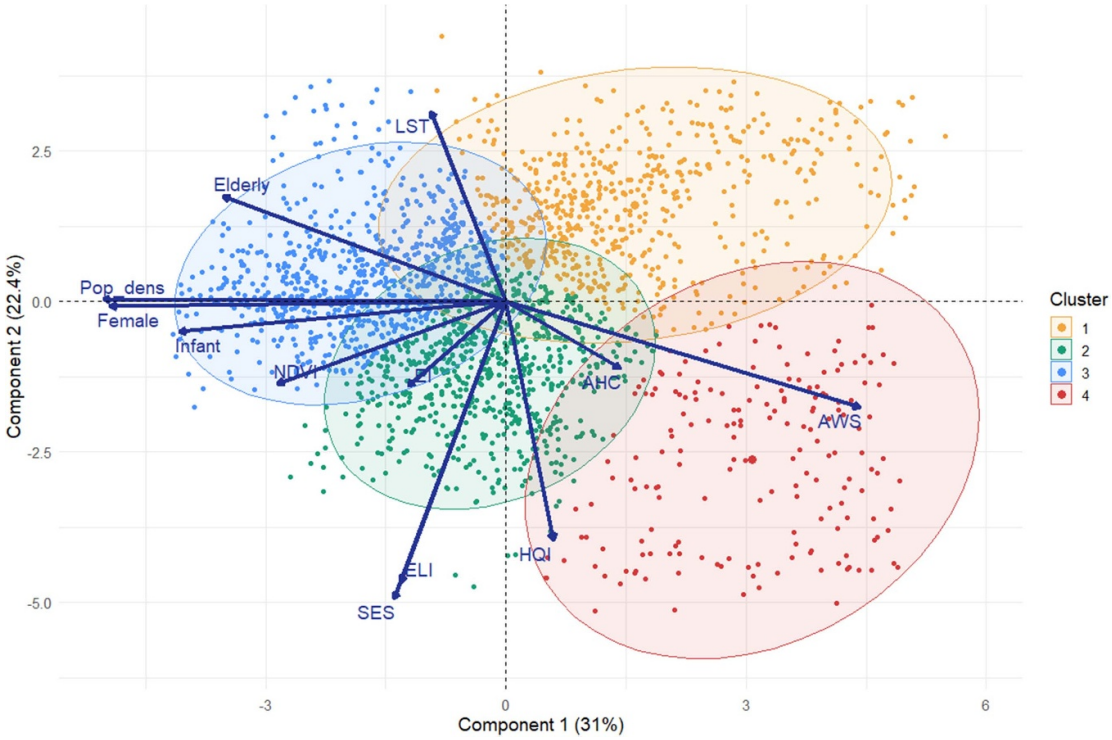

Figure 8. Principal-component biplot (Components 1 and 2) of heat-vulnerability indicators.

either isolated from the sea breeze or situated on the plateau, suggesting priority targets for cooling interventions and tailored social measures.

3.4. Hot-/cold-spots (Local Moran's I)

To refine the understanding of heat vulnerability, we carried out a local spatial association analysis (figures 11 and 12) in which each census block was weighted by its neighbors within an 800 m radius. Compared with the original HVI map (figure 10), these new maps reveal statistically coherent hot and cold spots that were previously less evident. High–high clusters (pink, indicating high vulnerability) align along the built corridor of Iquique from Arturo Prat through Hospital to Caupolicán, and they also appear in central Alto Hospicio and Pampa del Molle, confirming that the most vulnerable tracts are surrounded by similarly vulnerable neighbors. In contrast, extensive low–low clusters (light blue) trace the cooler and more affluent coastal fringe of Iquique, in Puerto, Cavancha and Playa Brava; and extend into Santa Rosa and the Autódromo sector of Alto Hospicio, marking contiguous areas of consistently low vulnerability. Two types of spatial outliers are also evident: Low–high tracts (blue), such as Barrio Industrial and parts of the north-eastern plateau, where a vulnerable tract is embedded in a low-vulnerability setting, and high–low tracts (red) scattered along the inland edge of Iquique, where relatively resilient blocks are surrounded by more vulnerable neighbors. Grey polygons represent areas without 2017 census data and were excluded from the analysis. Overall, incorporating the 800 m neighborhood structure sharpens the spatial pattern and helps identify consolidated hotspots that should be prioritized for cooling and social interventions, as well as isolated anomalies that may require different management strategies.

3.5. Coupling HVI with LCZ typologies

The final stage of the study links the HVI to LCZs. Figure 13 displays this relationship for LCZ classes 1–10, indicating the share of each built form that falls within each HVI level. Four main patterns emerge. First, the open and sparsely built categories, LCZ 4, 5, 6 and 10, are dominated by the very low vulnerability class, with more than ninety percent of their area showing minimal risk. Second, the compact high-rise and mid-rise fabrics, LCZ 1 and 2, exhibit the greatest internal diversity. About forty percent of their extent lies in the Low or Medium-Low classes, yet they also contain the largest fractions of medium-high, high and very high values, confirming that dense construction can magnify thermal and social risk when adaptive capacity is limited. Third, the compact low-rise LCZ 3 shows an intermediate profile: medium-low and medium together account for roughly forty-five percent of its surface,

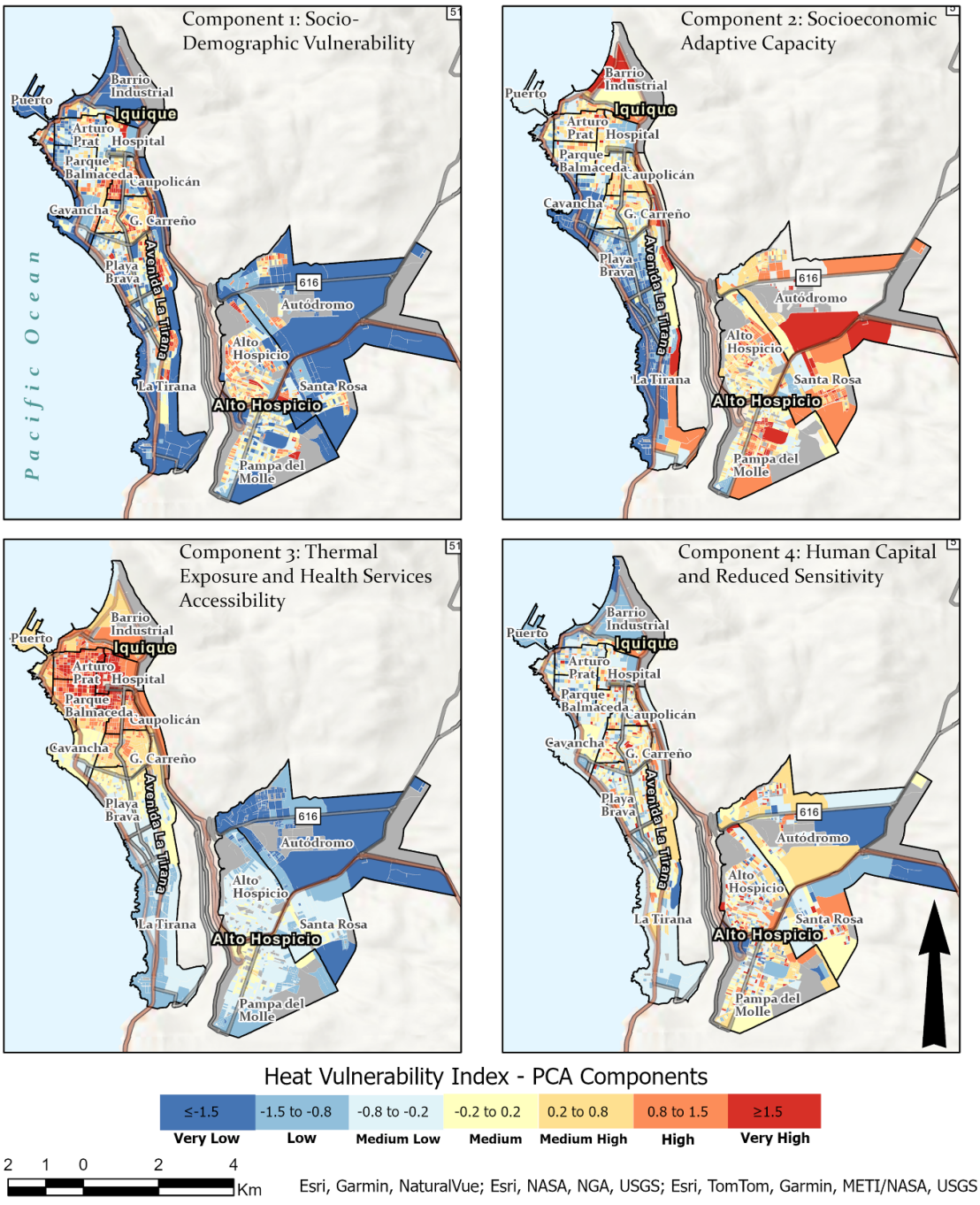

Figure 9. HVI spatial distribution according to each of the PCA.

while high and very high still exceed ten percent, indicating persistent vulnerability in older, tightly knit neighborhoods. Finally, LCZ 7, which corresponds to lightweight low-rise settlements, presents the most balanced distribution, with nearly one third of its area in medium-low to medium-high classes and a small though noticeable share in the very high category, reflecting the varied socio-economic conditions typical of informal or gradually formalized areas. Overall, the diagram suggests that vulnerability is lowest in open or vegetated morphologies and rises as built form becomes more compact, although the specific social context modulates the extent to which compact urban structures translate into critical HVI levels. LCZ 8 acts as an intermediate case: roughly 90% of its area falls within the very low, low, or medium-low HVI classes, whereas the medium-high to very high classes together account for only about 10%. This pattern places LCZ 8 closer to the open, low-density LCZs than to the compact high-density categories.

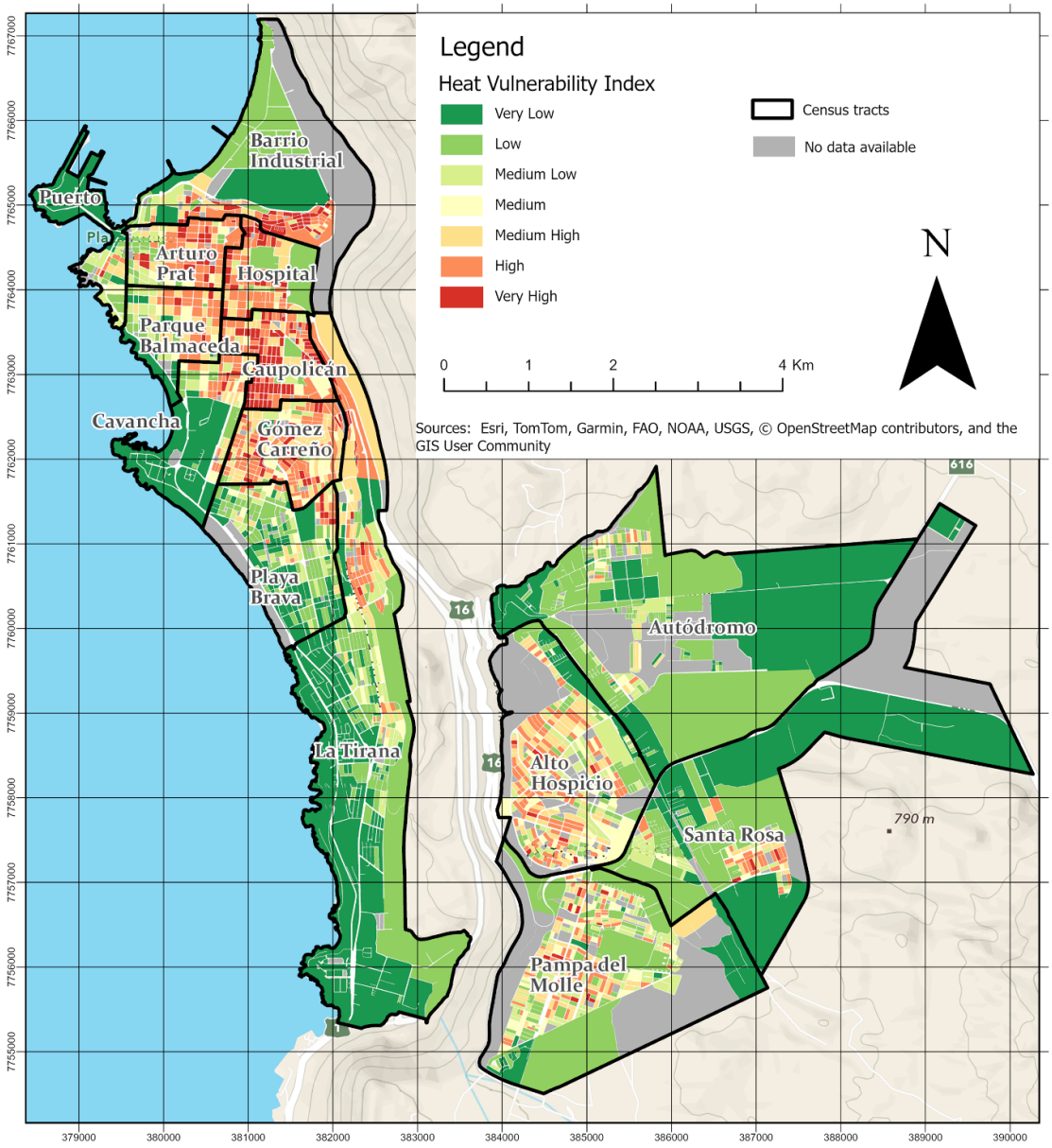

Figure 10. Heat vulnerability index by census tract in the Iquique–Alto Hospicio conurbation, 2019–2023.

4. Discussion and conclusions

4.1. Main findings on heat exposure in a hyper-arid coastal conurbation

Our multi-scale analysis confirms that Iquique–Alto Hospicio displays the dual SUHI behavior typical of other arid and semi-arid cities (Gourfi *et al* 2022, Chen *et al* 2023). By day, the upper-plateau municipality often acts as a SUCI, whereas the coastal strip registers weak-to-moderate positive anomalies. At night this pattern reverses: both cities develop an intense SUHI whose hotspots coincide with the densest and most impervious census blocks (figures 5–7). Downscaling to 10 m shows that intra-urban thermal gradients (∼7 °C) are an order of magnitude larger than the average city-to-rural contrast captured at MODIS resolution. Such fine-scale heterogeneity is crucial for heat-risk management because exposure can change drastically within a few blocks, a pattern also observed in Las Vegas (Fan *et al* 2017), Marrakech (Gourfi *et al* 2022), and Arica (Smith *et al* 2021). Managing a conurbation with such an elevation range remains challenging; future work should incorporate urban weather-station networks. Nevertheless, our results are robust across spatial scales.

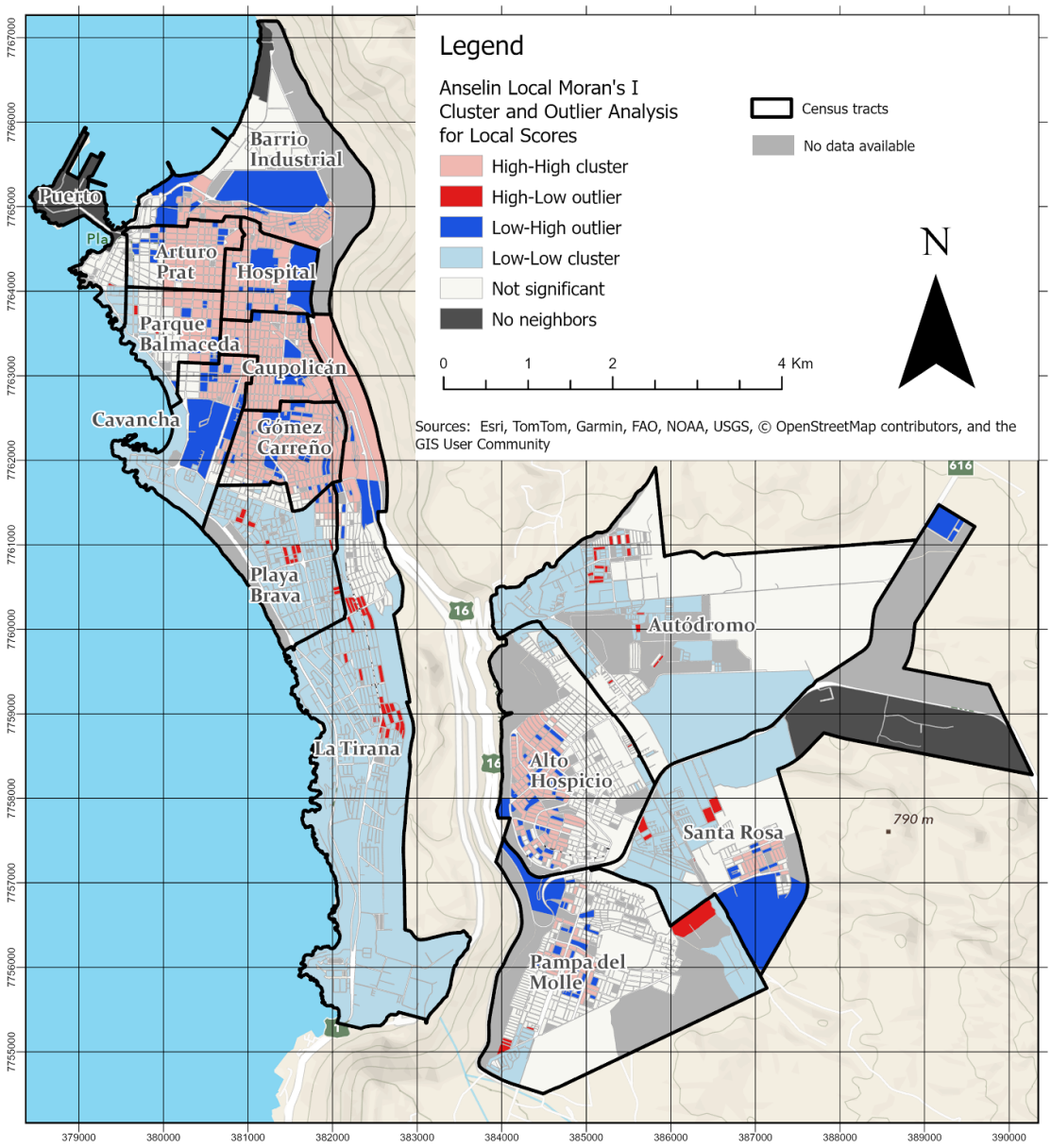

Figure 11. Local Moran's I cluster and outlier map of the heat-vulnerability index calculated with an 800 m spatial lag.

4.2. Coupling thermal exposure with socio-spatial vulnerability

The composite HVI reveals a coastal paradox: the historic center of Iquique, largely cooled by sea breezes, emerges as the main vulnerability hotspot because high demographic sensitivity and low adaptive capacity outweigh the presumed thermal relief. Conversely, several districts on the Alto Hospicio plateau combine moderate surface temperatures with limited social and human capital, producing medium-to-high vulnerability. This decoupling between heat exposure and social disadvantage mirrors findings for Guangzhou (Chen *et al* 2023) and Barcelona (García-Sierra and Domene 2022), underscoring that thermal metrics alone underestimate vulnerability and potential risk. Our results confirm that heat vulnerability is not determined solely by exposure to high land-surface temperatures but also by deeper socio-economic dimensions, such as limited adaptive resources, employment instability, and uneven access to water and health services, which amplify residents' sensitivity to heat.

4.3. The role of urban form: evidence from LCZs

Linking HVI scores with LCZ typologies (figure 13) clarifies how built morphology modulates vulnerability and risk, defining distinct morpho-climatic domains. Open residential forms (LCZ 4, 5 and 6) and low-rise warehouses (LCZ 10) maintain very-low HVI values, whereas compact low-, mid-, and high-rise zones (LCZ 1, 2 and 3) span the entire vulnerability spectrum, results consistent with Paris (Ma

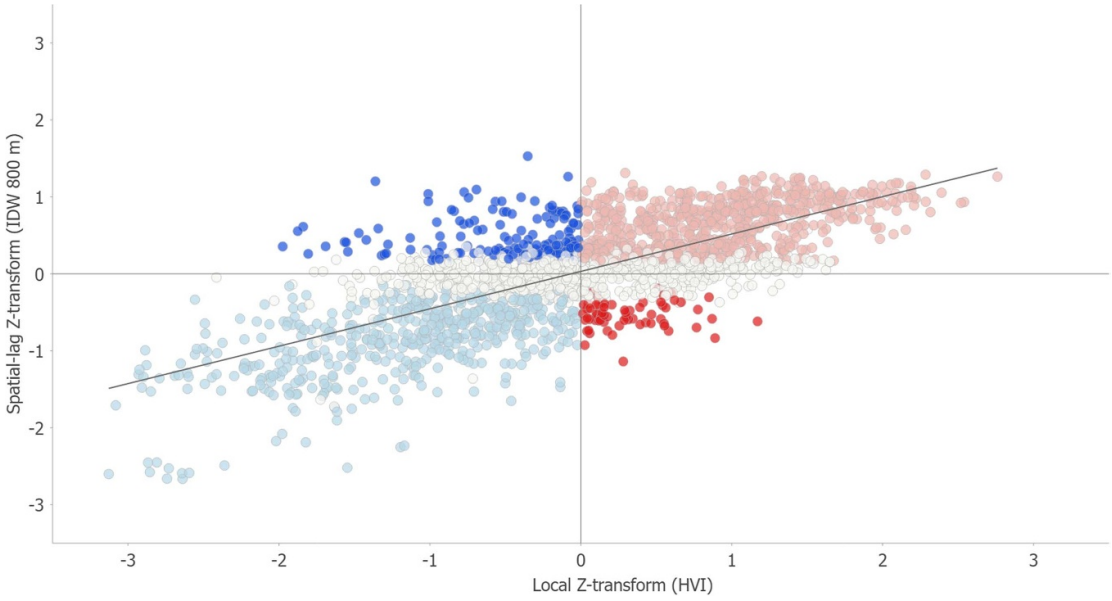

Figure 12. Moran scatterplot for the heat vulnerability index (HVI): Local Z-score transform (x-axis) versus inverse-distance–weighted spatial-lag Z-score transform at 800 m (y-axis). The slanted line represents the global Moran correlation. Dots are color-coded by statistically significant LISA clusters at $p < 0.05$: **High–High** (pink, high vulnerability surrounded by high vulnerability), **Low–Low** (light blue, low vulnerability surrounded by low vulnerability), and spatial outliers **Low–High** (blue) and **High–Low** (red). Points in white denote census block with average HVI values whose spatial association is not significant ($p > 0.05$).

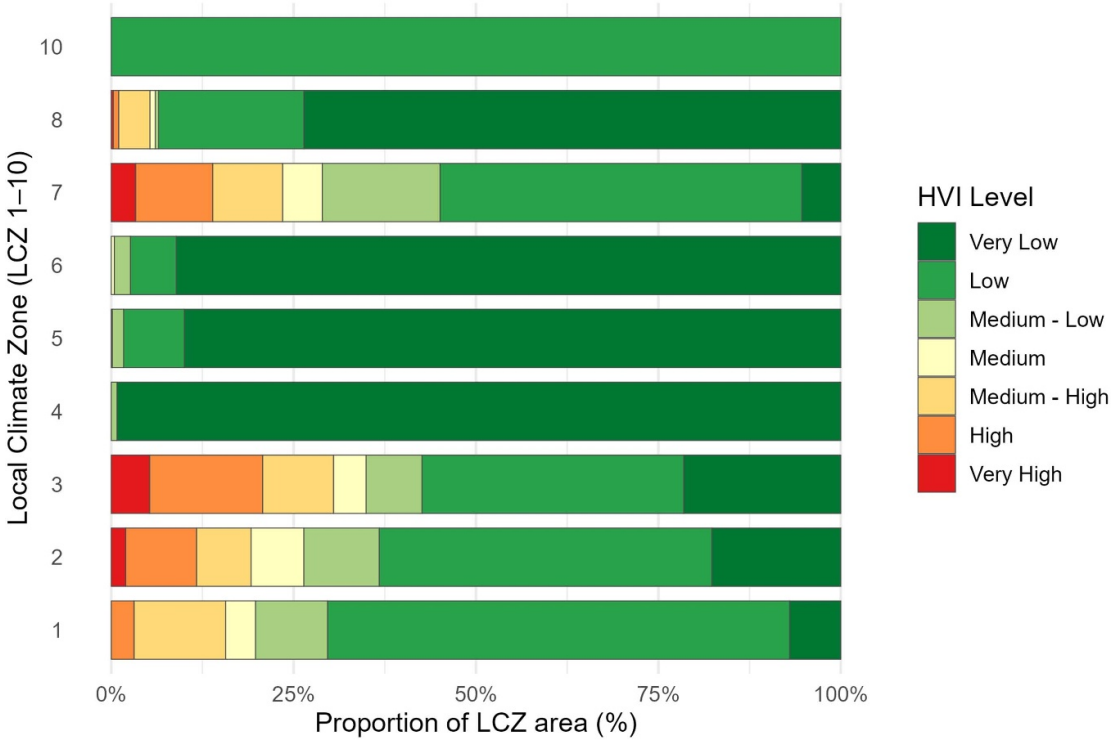

Figure 13. Heat-vulnerability distribution across LCZs.

et al 2024) and Shenyang (Zou *et al* 2025). The internal heterogeneity of LCZ 1–2 indicates that densification alone does not determine heat vulnerability; contextual adaptive capacity (e.g. housing quality, health-care access) modulates outcomes. While the LCZ framework captures the morphological heterogeneity that modulates surface heat, it only partially reflects social vulnerability. Some morphologies, such as lightweight low-rise or transitional compact zones, exhibit mismatches between structural form and observed vulnerability, highlighting the limits of LCZ typologies when socio-economic disparities

are strong (He *et al* 2024). Refining the classification or integrating socio-demographic weighting could enhance the model's capacity to capture these interactions (Fu *et al* 2024). Informal areas typical of Alto Hospicio show very-high vulnerability, and the transition from LCZ-7 to LCZ-3 suggests that piecemeal formalization without parallel investment in green-blue infrastructure can inadvertently maintain or worsen heat risk.

4.4. Implications for climate-resilient planning

Our findings point to three complementary urban-policy avenues for reducing thermal exposure and vulnerability: (1) targeted cooling interventions, in which hotspots identified with Local Moran's I guide the prioritized installation of cool roofs, pocket parks, or shaded corridors (Broadbent *et al* 2022), benefiting the greatest number of residents; (2) climate-sensitive zoning, whereby future densification follows LCZ-specific guidelines, for example, mandating ventilation corridors in compact mid- and high-rise zones (LCZ 1–2) and preserving vegetated or cool-pavement buffers around compact low-rise housing (LCZ 3) to mitigate nighttime heat retention; and (3) socially attuned heat-action plans that integrate HVI maps into early-warning systems and designate climate shelters such as libraries, shaded public green squares, and community centers in highly vulnerable areas, adapting the Barcelona 'climate-shelter' model to Chile's desert context.

4.5. Limitations and uncertainties

Several caveats merit attention. (i) Land-surface temperature is an imperfect proxy for air temperature, despite its utility in areas with sparse meteorological networks; validation with dense sensor arrays would refine exposure estimates. (ii) Census-tract aggregation masks social heterogeneity, and ongoing demographic shifts require continuous updates of exposure, sensitivity, and adaptive-capacity variables. (iii) Robust-linear downscaling inherits both radiometric noise and predictor uncertainty; future research should compare this method with machine-learning alternatives such as random forests or convolutional neural networks. (iv) The estimation of SUHI magnitude remains sensitive to the definition of rural reference zones—a well-documented source of uncertainty (Fu *et al* 2024)—particularly in regions with strong elevation gradients such as Iquique–Alto Hospicio, where separate coastal and plateau baselines were required to minimize lapse-rate bias. (v) Finally, the cross-sectional HVI omits adaptive dynamics, e.g. household acclimatization or municipal investments, that may evolve over coming decades (Craft and Fisher 2016). In addition, some relevant social dimensions, such as public health status, neighborhood cohesion, and institutional response capacity, were not explicitly included due to data unavailability, yet they likely play a critical role in shaping local vulnerability patterns and deserve further investigation.

4.6. Concluding remarks

This study provides the first integrated, high-resolution assessment of thermal exposure and socio-spatial vulnerability for the rapidly growing conurbation of Iquique–Alto Hospicio. By combining MODIS surface-temperature climatologies with Sentinel-2-based downscaling, we produced an HVI suitable for neighborhood-scale planning. Principal-component analysis proved effective in defining the composite components, and coupling the HVI with Local Moran's I highlighted priority intervention areas. Using the LCZ framework, we show that where people live, and how neighborhoods are built, matters as much as the ambient heat itself. The sharp coastal-to-plateau gradients and intra-urban mosaics documented here demand differentiated, equity-centered adaptation strategies. As global warming intensifies heat extremes, the evidence presented for Iquique–Alto Hospicio offers a transferable framework for hyperarid coastal cities worldwide committed to climate-resilient futures. Our results also align with recent methodological advances emphasizing that the reliability of SUHI assessments depends on context-specific reference definitions and terrain adjustments (Fu *et al* 2024), reinforcing the transferability of our two-tier rural baseline approach to other topographically complex or coastal–inland urban systems.

Data availability statement

The data that support the findings of this study are openly available from multiple sources. MODIS and Sentinel datasets were accessed and processed through the Google Earth Engine platform. Socio-demographic and infrastructural indicators were obtained from the *Instituto Nacional de Estadísticas de Chile* (INE) via its Open Geodata Portal (www.ine.gob.cl/herramientas/portal-de-mapas/geodatos-abiertos), and from the *Observatorio de Bienestar Territorial* at Universidad Adolfo Ibáñez (https://matrizbht.cl/). All derived datasets, including downscaled LST layers, Heat Vulnerability Index (HVI)

indicators, and Local Climate Zone (LCZ) shapefiles, are openly available in Zenodo under a CC-BY 4.0 license at the following URL/DOI: https://doi.org/10.5281/zenodo.17313354.

Acknowledgments

This study was supported by the Chilean National Agency for Research and Development (ANID) through FONDECYT Project No. 1221688 and by the Center for Climate and Resilience Research (CR)^2 (ANID/FONDAP/1522 A0002). R.S.N. is supported by grant RYC2021-034330-I funded by MCIN/AEI/10.13039/501100011033 and by 'European Union NextGenerationEU/PRTR'. We gratefully acknowledge the Moderate Resolution Imaging Spectroradiometer (MODIS) mission, operated by NASA and the U.S. Geological Survey (USGS), and the Sentinel program, operated by the European Space Agency (ESA) under the Copernicus initiative, for providing open-access satellite data. We also thank the Google Earth Engine platform for enabling large-scale data access, processing, and analysis.

Author contributions

Pablo Sarricolea 0000-0002-6679-2798
Conceptualization (lead), Data curation (equal), Formal analysis (lead), Funding acquisition (lead), Investigation (equal), Methodology (equal), Resources (lead), Supervision (equal), Validation (equal), Visualization (equal), Writing – original draft (lead), Writing – review & editing (equal)

Alexis Baltazar 0000-0002-5294-6717
Formal analysis (equal), Investigation (equal), Methodology (equal), Writing – original draft (equal)

Oliver Meseguer-Ruiz 0000-0002-2222-6137
Conceptualization (equal), Investigation (equal), Writing – original draft (equal), Writing – review & editing (equal)

Pamela Smith 0000-0001-9355-9601
Conceptualization (equal), Investigation (equal), Methodology (equal), Writing – review & editing (equal)

Natasha Picone 0000-0001-6183-0401
Conceptualization (equal), Methodology (equal), Writing – original draft (equal), Writing – review & editing (equal)

Roberto Serrano-Notivoli 0000-0001-7663-1202
Investigation (equal), Methodology (equal), Writing – original draft (equal), Writing – review & editing (equal)

Paulina Vidal-Paez 0000-0003-1836-5684
Investigation (equal), Methodology (equal), Writing – original draft (equal), Writing – review & editing (equal)

Magdalena Fuentealba 0000-0003-2321-6069
Investigation (equal), Writing – original draft (equal), Writing – review & editing (equal)

Felipe Thomas 0000-0002-5851-8756
Data curation (equal), Methodology (equal), Writing – original draft (equal), Writing – review & editing (equal)

References

Anselin L 1995 Local indicators of spatial association—LISA *Geog. Anal.* **27** 93–115
Broadbent A M, Declet-Barreto J, Krayenhoff E S, Harlan S L and Georgescu M 2022 Targeted implementation of cool roofs for equitable urban adaptation to extreme heat *Sci. Total Environ.* **811** 151326
Carter V G *et al* 2025 Even desert cities could pull drinking water from the air: fog harvesting potential in Alto Hospicio, Chile *Front. Environ. Sci.* **13** 1537058
Chen G, Chen Y, He H, Wang J, Zhao L and Cai Y 2023 Assessing the synergies between heat waves and urban heat islands of different local climate zones in Guangzhou, China *Build. Environ.* **240** 110434
Chen Y, Xie M, Chen B, Wang H and Teng Y 2022 Surface regional heat (Cool) island effect and its diurnal differences in arid and semiarid resource-based urban agglomerations *Chin. Geogr. Sci.* **33** 131–43
Coffel E D, Horton R M and de Sherbinin A 2017 Temperature and humidity based projections of a rapid rise in global heat stress exposure during the 21st century *Environ. Res. Lett.* **13** 014001

Craft B and Fisher S 2016 Measuring effective and adequate adaptation (International Institute for Environment and Development) (available at: www.iied.org/10171iied)
Cutter S L, Boruff B J and Shirley W L 2003 Social vulnerability to environmental hazards *Soc. Sci. Q.* **84** 242–61
Cutter S L, Burton C G and Emrich C T 2010a Disaster resilience indicators for benchmarking baseline conditions *J. Homel. Secur. Emerg. Manage.* **7** 1–22
Cutter S L, Mitchell J T and Scott M S 2010b Revealing the vulnerability of people and places: a case study of Georgetown County, South Carolina *Ann. Assoc. Am. Geogr.* **90** 713–37
Fan C, Myint S, Kaplan S, Middel A, Zheng B, Rahman A, Huang H, Brazel A and Blumberg D 2017 Understanding the impact of urbanization on surface urban heat islands—a longitudinal analysis of the oasis effect in subtropical desert cities *Remote. Sens* **9** 672
Fu X, He B-J and Liu H 2024 Uncertainties of urban heat island estimation with diverse reference delineation method based on urban-rural division and local climate zone *IEEE J. Sel. Top. Appl. Earth Obs. Remote Sens.* **17** 18818–33
Fuladlu K 2022 Thermal response to land-use land-cover patterns: an experimental study in Famagusta, Cyprus *CLEAN–Soil, Air, Water* **50** 2100284
Fuladlu K 2024 Human activities and increased anthropogenic emissions: a remote sensing study in Cyprus *Environ. Dev.* **51** 101023
Garcia-Sierra M and Domene E 2022 La calor en un futur: Índex de vulnerabilitat al canvi climàtic (IVAC) (Institut d'Estudis Regionals i Metropolitans de Barcelona) (available at: www.institutmetropoli.cat/wp-content/uploads/2023/03/5.3.1.Lacalorenunfutur_IVAC_set2022.pdf)
Georgi B, Isoard S, Asquith M, Garzillo C, Swart R J and Timmerman J G 2016 *Urban adaptation to climate change in Europe 2016 — Transforming cities in a changing climate 12* (European Environment Agency) (available at: www.eea.europa.eu/en/analysis/publications/urban-adaptation-2016)
Gourfi A, Taïbi A, Salhi S, Hannani M and Boujrouf S 2022 The surface urban heat island and key mitigation factors in arid climate cities, case of Marrakesh *Morocco. Remote. Sens.* **14** 3935
Haashemi S, Weng Q, Darvishi A and Alavipanah S 2016 Seasonal variations of the surface urban heat island in a semi-arid city *Remote. Sens.* **8** 352
Harlan S L, Brazel A J, Prashad L, Stefanov W L and Larsen L 2006 Neighborhood microclimates and vulnerability to heat stress *Soc. Sci. Med.* **63** 2847–63
He B-J, Fu X, Zhao Z, Chen P, Sharifi A and Li H 2024 Capability of LCZ scheme to differentiate urban thermal environments in five megacities of China: implications for integrating LCZ system into heat–resilient planning and design *IEEE J. Sel. Top. Appl. Earth Obs. Remote Sens.* **17** 18800–17
Inostroza L, Palme M, De La Barrera F and Shaman J 2016 A heat vulnerability index: spatial patterns of exposure, sensitivity and adaptive capacity for Santiago de Chile *PLoS One* **11** e0162464
Johnson D P, Stanforth A, Lulla V and Luber G 2012 Developing an applied extreme heat vulnerability index utilizing socioeconomic and environmental data *Appl. Geogr.* **35** 23–31
Kaiser H F 1960 The application of electronic computers to factor analysis *Educ. Psychol. Meas.* **20** 141–51
Lai W, Li S, Liu Y and Barwick P J 2022 Adaptation mitigates the negative effect of temperature shocks on household consumption *Nat. Human Behav.* **6** 837–46
Limaye V S and Males J 2023 The hidden health costs of climate change: accounting for extreme heat harms to women in the global South *PLoS Clim.* **2** e0000267
Liu H and Weng Q 2018 Scaling effect of fused ASTER-MODIS land surface temperature in an urban environment *Sensors* **18** 4058
Liu S, Wang Y, Gong P, Zhang G J, Li X, Zhao Y, Wang P, Zhou J, Zhou X and Yu L 2025 Regional warming from urbanization is disproportionate to urban expansion rate *One Earth* **8** 101234
Luo S, Gu X, Guan Y, Zheng Y, Wang L, Zhang X, Cao Q, Kong D and Li J 2024 Anthropogenic climate change and urbanization exacerbate risk of hybrid heat extremes in China *J. Geophys. Res. Atmos.* **129** e2024JD041568
Ma L, Huang G, Johnson B A, Chen Z, Li M, Yan Z, Zhan W, Lu H, He W and Lian D 2023 Investigating urban heat-related health risks based on local climate zones: a case study of Changzhou in China *Sustain. Cities Soc.* **91** 104402
Ma X, Miao S, Masson V, Wurtz J, Zhang Y, Wang J, Huang X-Y and Yan C 2024 The synergistic effects of urbanization and an extreme heatwave event on urban thermal environment in Paris *Urban Clim.* **53** 101785
Maier G, Grundstein A, Jang W, Li C, Naeher L P and Shepherd M 2014 Assessing the performance of a vulnerability index during oppressive heat across Georgia, United States *Weather Clim. Soc.* **6** 253–63
Manoli G, Fatichi S, Schläpfer M, Yu K, Crowther T W, Meili N, Burlando P, Katul G G and Bou-Zeid E 2019 Magnitude of urban heat islands largely explained by climate and population *Nature* **573** 55–60
Martín Y and Paneque P 2022 Moving from adaptation capacities to implementing adaptation to extreme heat events in urban areas of the European Union: introducing the U-ADAPT! research approach *J. Environ. Manage.* **310** 114773
Mhawej M and Abunnasr Y 2022 Towards a daily 10-m land surface temperature product: the Google Earth Engine Daily Ten-ST-GEE system *Comput. Geosci.* **161** 105069
Mora C *et al* 2017 Global risk of deadly heat *Nat. Clim. Change* **7** 501–6
Niu Y, Li Z, Gao Y, Liu X, Xu L, Vardoulakis S, Yue Y, Wang J and Liu Q 2021 A systematic review of the development and validation of the heat vulnerability index: major factors, methods, and spatial units *Curr. Clim. Change Rep.* **7** 87–97
Olivares A *et al* 2025 Heat vulnerability index mapping through principal component analysis and equal weight methods: comparing Spatial patterns at a low urban scale and local climate zones in an arid mid-size South American coastal city *Nat. Hazards* **121** 13447–73
Palme M, Inostroza L, Villacreses G, Carrasco C and Henríquez C 2019 Urban climate in the South American coastal cities of Guayaquil, Lima, Antofagasta, and Valparaíso, and its impacts on the energy efficiency of buildings *Urban Climates in Latin America* (Springer) eds E C Henríquez and H Romero pp 33–62
Quintana-Talvac C, Corvacho-Ganahin O, Smith P, Sarricolea P, Prieto M and Meseguer-Ruiz O 2021 Urban heat islands and vulnerable populations in a mid-size coastal city in an arid environment *Atmosphere* **12** 917
Reid C E *et al* 2012 Evaluation of a heat vulnerability index on abnormally hot days: an environmental public health tracking study *Environ. Health Perspect.* **120** 715–20
Reid C E, O'Neill M S, Gronlund C J, Brines S J, Brown D G, Diez-Roux A V and Schwartz J 2009 Mapping community determinants of heat vulnerability *Environ. Health Perspect.* **117** 1730–6
Romero-Lankao P, Qin H and Dickinson K 2012 Urban vulnerability to temperature-related hazards: a meta-analysis and meta-knowledge approach *Glob. Environ. Change* **22** 670–83

Sarricolea P, Herrera-Ossandón M and Meseguer-Ruiz Ó 2017 Climatic regionalisation of continental Chile *J. Maps* **13** 66–73
Sarricolea P, Smith P, Romero-Aravena H, Serrano-Notivoli R, Fuentealba M and Meseguer-Ruiz O 2022 Socioeconomic inequalities and the surface heat island distribution in Santiago, Chile *Sci. Total Environ.* **832** 155152
Shahfahad, Bindajam S, Bindajam A A, Naikoo M W, Horo J, Mallick J, Rihan M, Malcoti M D, Talukdar S, Rahman R and Rahman A 2023 Response of soil moisture and vegetation conditions in seasonal variation of land surface temperature and surface urban heat island intensity in sub-tropical semi-arid cities *Theor. Appl. Climatol.* **153** 367–95
Smith P, Peralta O, Sarricolea P, Thomas F and Meseguer-Ruiz O 2023 Climate-sensitive planning: opportunities through the study of LCZs in Chile. opportunities through the study of LCZs in Chile *Build. Environ.* **242** 110444
Smith P, Sarricolea P, Peralta O, Águila J P and Thomas F 2021 Study of the urban microclimate using thermal UAV: the case of the mid-sized cities of Arica (arid) and Curicó (Mediterranean), Chile *Build. Environ.* **206** 108372
Stewart I D and Oke T R 2012 Local climate zones for urban temperature studies *Bull. Am. Meteorol. Soc.* **93** 1879–900
Sun Y, Hu T and Zhang X 2018 Substantial increase in heat wave risks in China in a future warmer world *Earth's Future* **6** 1528–38
Tuholske C, Caylor K, Funk C, Verdin A, Sweeney S, Grace K, Peterson P and Evans T 2021 Global urban population exposure to extreme heat *Proc. Natl Acad. Sci.* **118** e2024792118
van Steen Y, Ntarladima A-M, Grobbee R, Karssenberg D and Vaartjes I 2019 Sex differences in mortality after heat waves: are elderly women at higher risk? *Int. Arch. Occup. Environ. Health* **92** 37–48
Wang J *et al* 2021 Anthropogenic emissions and urbanization increase risk of compound hot extremes in cities *Nat. Clim. Change* **11** 1084–9
Wang J, McPhearson T, Zhou W, Cook E M, Herreros-Cantis P and Liu J 2023 Comparing relationships between urban heat exposure, ecological structure, and socio-economic patterns in Beijing and New York City *Landsc. Urban Plann.* **235** 104750
Wang L, Di J, Wang Q, Zhang H, Zhao W, Shi X, Di Q, Ji J S, Liang W and Huang C 2024 Heat exposure induced risks of preterm birth mediated by maternal hypertension *Nat. Med.* **30** 1974–81
Wei X, Eboy O V, Cao G and Xu L 2023 Spatio-temporal variation of water conservation and its impact factors on the southern slope of Qilian Mountains *Reg. Sustain.* **4** 54–67
Wouters H, De Ridder K, Poelmans L, Willems P, Brouwers J, Hosseinzadehtalaei P, Tabari H, Vanden Broucke S, Van lipzig N P M and Demuzere M 2017 Heat stress increase under climate change twice as large in cities as in rural areas: a study for a densely populated midlatitude maritime region *Geophys. Res. Lett.* **44** 8997–9007
Wu S, Wang P, Tong X, Tian H, Zhao Y and Luo M 2021 Urbanization-driven increases in summertime compound heat extremes across China *Sci. Total Environ.* **799** 149166
Yang X, Xu X, Wang Y, Yang J and Wu X 2024 Heat exposure impacts on urban health: a meta-analysis *Sci. Total Environ.* **947** 174650
Zhang R, Yang J, Ma X, Xiao X and Xia J 2023 Optimal allocation of local climate zones based on heat vulnerability perspective *Sustain. Cities Soc.* **99** 104981
Zhou S, Zheng H, Liu X, Gao Q and Xie J 2023 Identifying the effects of vegetation on urban surface temperatures based on urban–rural local climate zones in a subtropical metropolis *Remote Sensing* **15** 4743
Zhou Y, Larochelle L, Khan F A and Pilote L 2025 Sex differences in the impact of extreme heat on cardiovascular disease outcomes: a systematic review and meta-analysis *Environ. Health* **24** 20
Zou Q, Yang J, Zhang Y, Bai Y and Wang J 2025 Variation in community heat vulnerability for Shenyang City under local climate zone perspective *Build. Environ.* **267** 112242